Online Materials and Methods

Cell culture

We isolated SMCs enzymatically from the explants of ascending aortas from 136 healthy heart transplant donors (118 males and 33 females) at the University of California at Los Angeles (UCLA) transplant program as described previously[27]. These cells were readily accessible from the discarded pieces of ascending aortas of the transplanted hearts. We also purchased aortic SMCs isolated from ascending aortas from 15 donors from Lonza and PromoCell. We maintained the cells in Smooth Muscle Cell Basal Medium (SmBM, CC-3181, Lonza) supplemented with Smooth Muscle Medium-2 SingleQuots Kit (SmGM-2, CC-4149, Lonza) (complete media). We cultured the SMCs in complete media (containing 5% FBS) until 90% confluence. We then switched to either serum-free media to mimic the quiescent state of SMCs or continued to culture in complete media to mimic the proliferative state of SMCs for 24 hours[28,29]. We harvested the cells in Qiazol and extracted total RNA. The Institutional Review Boards of UCLA and the University of Virginia approved this study.

Genotyping and ancestry determination

We genotyped the donors using the Illumina Multi-Ethnic Global genotyping array for 1.8 million single nucleotide polymorphisms (SNPs). We pruned the SNPs based on call rate (< 2%), Hardy-Weinberg equilibrium ($P_{HWE}<1x10^{-6}$), and minor allele frequency (< 5%), and imputed non-genotyped SNPs using the 1000 Genomes Phase 3 reference panel of 2,504 individuals from 26 populations[30] using Michigan Imputation Server [31]. After removing the SNPs with minor allele frequency less than 5% and imputation quality less than 0.3, we were left with ~6.3 million SNPs for association studies. To determine the ancestral background of the donors, we excluded SNPs in regions of extended high linkage disequilibrium (LD) and pruned the remaining SNPs at an LD threshold $r^2 \geq 0.2$. We clustered the filtered genotypes with the genotypes of 12 populations represented in the 1000 Genomes Phase 3 data[30] with principal component analysis (PCA) implemented in KING[32].

RNA extraction, sequencing, mapping and quantification

We performed the sequencing of the ribosomal RNA-depleted total RNA isolated from SMCs of the 151 donors cultured in the presence or absence of 5% FBS. Total RNA was extracted using the RNeasy Micro Kit (Qiagen) and the RNase-free DNase Set. RNA integrity scores for all samples, as measured by the Agilent TapeStation, were greater than 9, indicating high-quality RNA preparations. Sequencing libraries were prepared with the Illumina TruSeq Stranded mRNA Library Prep Kit and were sequenced to ~100 million read depth with 150 bp paired-end reads at the Psomogen sequencing facility. We trimmed the reads with low average Phred scores (<20) using Trim Galore and mapped the reads to the hg38 version of the human reference genome using the STAR Aligner in two-pass mode to increase the mapping efficiency and sensitivity[33]. We only retained the uniquely mapped read pairs. We quantified gene expression by calculating the transcripts per million (TPM) for each gene using RNA-SeQC[34] based on GENCODE v32 transcript annotations. In addition to protein-coding RNAs, we also measured the non-coding RNA since they have been shown to play significant roles in SMC biology[35]. We considered a

gene as expressed if it had more than 6 read counts and 0.1 TPM in at least 20% of the samples.

Sample swap identification

To detect sample swaps, we used NGSCheckMate[36] and verifyBamID[37] to call variants from RNA-seq data and assign the best matches between the RNA-seq and genotype data. This led to the removal of 11 and 6 samples from quiescent (without FBS) and proliferative (with FBS) SMC cultures, respectively.

Differential gene expression and functional enrichment analysis

We included 14,341 genes with > 6 reads in at least 80% of the samples in at least one of the two conditions for differential expression analysis using DESeq2[38]. We considered genes to be differentially expressed between proliferative and quiescent conditions when $P_{adj} < 3x10^{-3}$ and the absolute value of $\log_2$(fold-change)> 0.5. We identified the surrogate variables using the *svaseq* function in the *sva* package[39] using gene expression measured in TPM as input. We performed principal component analysis (PCA) of these surrogate variables using the ARSyNSeq function from the NOISeq package in R[40]. To characterize the functional consequences of gene expression changes associated with proliferative and quiescent conditions, we performed Gene Set Enrichment Analysis (GSEA) using Gene Ontology (GO) terms. We ranked the genes based on fold-change and differential expression between the two conditions (P_{adj}<0.05) and used GSEA on the ranked set of genes using all expressed genes in SMCs as background to perform GO enrichment analysis. We considered GO terms with FDR<0.05 as significantly enriched.

***Cis*-eQTL and -sQTL identification**

For *cis*-eQTL discovery, we conducted our analysis according to the GTEx pipeline to compare our eQTL results to the GTEx dataset[41], consisting of 838 donors and 17,382 samples from 52 tissues and two cell lines. Therefore, we considered the genes with sufficient expression level (TPM > 0.1 and read count > 6) in at least 20% of the samples. After filtering, we normalized the read counts using the trimmed mean of M values (TMM)[42] followed by inverse normalization. We corrected the gene expression data for technical artifacts and unknown technical confounders using the probabilistic estimation of expression residuals (PEER) framework[43]. To optimize for *cis*-eQTL discovery, we performed eQTL mapping using inverse normalized gene expression residuals corrected with 5, 10, 15, 20, 25, 30, 35, 40 or 45 PEER factors along with sex and 4 genotype principal components (PCs) using tensorQTL permutation pass analysis[44]. We implemented tensorQTL permutation testing to detect the top nominal associated SNP within 1 MB of the transcription start site (TSS) of a gene, defined as the *cis* region, and with a beta approximation to model the permutation result and correct for all SNPs in linkage disequilibrium (LD) with the most significant SNP (referred here as eSNP) per gene. We used the '--permute 1000 10000' option in tensorQTL. Beta approximated permutation *P*-values were then corrected for multiple testing using the q-value false discovery rate FDR correction[45]. A gene with a *cis*-eQTL (eGene) was defined by having an FDR q-value <0.05. We report the results of eQTL mapping for 30 and 35 PEER factors

for the quiescent and proliferative conditions, respectively since we discovered the maximum number of eQTL genes with that many PEER factors.

We utilized LeafCutter[46] to obtain and quantify clusters of variably spliced introns and tensorQTL to map sQTLs within a 200 KB window around splice donor sites, controlling for sex, four genotype PCs, and 6 and 8 PEER factors for quiescent and proliferative conditions, respectively. Unlike eQTL, we found that using 2, 4, 6, 8, 10 or 12 PEER factors were sufficient to optimize the number of sQTL. We identified secondary and beyond independent eQTLs and sQTLs by rerunning permutation tests in tensorQTL[44] for every gene or intron, respectively, conditioning on the primary eSNP. Conditional secondary and beyond molecular QTLs were considered significant if the FDR q-value <0.05. We used LocusZoom for the regional visualization of eQTL/sQTL results on the basis of linkage disequilibrium (LD) ascertained from the 151 donors in our study[47]. For pairwise gene set overlap comparisons, we employed the hypergeometric test. For overlaps that included eQTL genes, we used the maximal number of expressed genes as the background population size. For overlaps that included sQTL genes, we used the maximal number of expressed genes with more than one exon as the background population size. We reported probabilities that the number of overlaps were greater than or equal to the observed overlaps.

Detecting condition- and sex-biased eQTLs

To determine *cis*-eQTL SNPs with statistically significant differential effects on gene expression in quiescent or proliferative conditions, we first determined the SNP with the highest statistical significance per each *cis*-eQTL gene in either the quiescent or proliferative condition. We then tested if the effect sizes of the eSNP on the *cis*-eGene were significantly different between the two conditions using a Z-test utilizing the effect size (β) and its standard error (σ^2) as described previously[48]. We corrected the resulting *P*-values for multiple testing using the q-value false discovery rate FDR correction[45]. We determined a condition-specific eQTL if the FDR q-value in the Z-test was < 0.05. 90% confidence intervals of the effect size (β) were calculated for each condition. We considered an effect as positive if the confidence interval did not include 0 and the z-score was positive and an effect as negative if the confidence interval did not include 0 and the z-score was negative. We classified a condition-specific eQTL as condition-specific direction if the confidence intervals differed in sign, condition-specific magnitude if the confidence intervals were the same sign, and condition-specific effect if one of the confidence intervals included 0.

To determine *cis*-eQTL SNPs with statistically significant different effects on gene expression in males and females, we performed sex-biased *cis*-eQTL analysis on autosomal genes in quiescent and proliferative conditions separately. Like standard eQTL mapping, we first normalized read counts using the trimmed mean of M values and inverse normal transformed gene expression data. Next, we used a linear regression model including genotype, 4 genotype PCs, and the same number of PEER factors we used for standard eQTL mapping using tensorQTL, after removing the effect of sex, to test for significance of genotype-by-sex (G x Sex) interaction on expression. We applied eigenMT, a permutation method, that estimates the effective number of independent tests based on the local LD structure[49]. We considered a sex-biased *cis*-eQTL significant if the eigenMT value <0.05. To classify the identified sex-biased *cis*-eQTLs, we conducted

independent linear regression models for each sex-biased eQTL gene and eSNP pair, controlling for four genotype PCs and same number of PEER factors we used for sex-biased *cis*-eQTLs. Similar to condition-specific eQTL analysis, we calculated the 90% confidence intervals of the effect size (β) for each sex per condition. We separated the sex-biased eQTLs into three different categories: sex-biased effect, sex-biased direction, and sex-biased magnitude.

Overlap of SMC cis-eQTLs with GTEx cis-eQTLs and identification of SMC-specific eQTLs

To compare GTEx eQTLs with our SMC eQTLs we utilized the QTlizer R package[50] to query the significant SMC eSNPs and LD proxies ($r^2 \geq 0.8$) for eQTL signals in GTEx v8[41]. We only retained GTEx eQTL signals at 5% FDR across all the tissues. We used the variant and gene pairs as identifiers in both GTEx and SMC eQTL datasets. We considered any variant and gene pair significant novel if it was only present in our study. If it was found in any GTEx tissues and our study, we considered it as shared.

Additionally, we identified SMC-specific eQTLs with respect to the GTEx eQTL results[41]. For each SMC gene with an eQTL, we selected the most significantly associated SNP, and performed multi-tissue eQTL calling using all the available SNPs within 1 MB of the TSS of the all the genes in the GTEx dataset using METASOFT[51]. We calculated the posterior probability that the effect exists in each tissue as denoted by the m-value. We defined SMC-specific eQTLs as SNP-gene pairs with m-value>0.9 for SMCs and < 0.1 for all the GTEx tissues. We also queried the SMC-specific eQTLs identified by METASOFT for significant associations in the STARNET dataset[20].

Colocalization between molecular SMC QTLs and CAD GWAS signals

We examined whether each *cis*-eQTL and sQTL is colocalized with the GWAS loci associated with CAD using four different methods. We used the CAD GWAS meta-analysis from UK Biobank and CARDIoGRAMplusC4D, with a total of 122,733 cases and 424,528 controls of European ancestry. First, we calculated the linkage disequilibrium (LD) r^2 value between the GWAS index variant and the variant with the most significant association with expression or splice QTL (eSNP and sSNP) in our study population. We defined GWAS-coincident eQTLs/sQTLs as loci with pairwise LD $r^2 \geq 0.8$ (1000G EUR) between the GWAS index variant and the lead eSNP/sSNP. To evaluate the association between the GWAS variant and the lead eQTL variant at each locus, we performed conditional analyses; we tested the association between the index variant and transcript level when the lead GWAS SNP was included in the model. Second, we used Summary Level Mendelian Randomization (SMR)[52] to test for the pleiotropic association of gene expression in SMCs and CAD. We identified genome-wide significant eQTL and sQTL colocalizations based on their SMR *P*-values after controlling false discoveries. For the eQTL analysis, we performed a SMR test on genes with a *cis*-eQTL *P*-value < 1.42×10^{-5} and 1.69×10^{-5}, corresponding to 5% FDR, in the quiescent and proliferative datasets, for a total of 2,228 and 3,090 tests, respectively. For the sQTL datasets, we used a *P*-value cutoff of 1.73×10^{-5} and 3.08×10^{-5} for a total of 6,787 and 7,945 SMR tests in the quiescent and proliferative sQTL datasets, respectively. We used the 1000 Genomes European reference panel to account for linkage disequilibrium. We considered loci with an adjusted SMR *P*-value (5% FDR) to have evidence of colocalization. Third, we used eQTL and

GWAS CAusal Variants Identification in Associated Regions (eCAVIAR)[53], to test for causal SNPs between our eQTL and sQTL data and the CAD GWAS considering variants within a 500 kb and 200 kb window around the eSNP for each eGene or sGene, respectively. The maximum number of causal variants was set to 2 and variants were considered colocalized if the colocalization posterior probability (CLPP) was greater than 0.01. Finally, we implemented Bayesian Colocalization Analysis using Bayes Factors (COLOC) using the R package COLOC[54]. We first selected SNPs in each CAD GWAS locus with genome-wide significance, and then created 200 KB windows around significant SNPs. Following this, we merged nearby windows (>100 KB distance) together to form loci. We input these loci into COLOC with the default priors ($p1/p2 = 1 \times 10^{-4}$, and $p12 = 1 \times 10^{-5}$), and considered a locus colocalized if PPH4, the hypothesis of a single shared causal variant for both traits within a window, was greater than 0.50. We then plotted and visually inspected all analyzed loci using LocusCompare[55]. Loci that passed both visual inspection and colocalization criteria were considered colocalized.

Identification of accessible chromatin regions in SMCs and transcription factor binding site analysis

We performed transposase-accessible chromatin with high-throughput sequencing (ATACseq) in SMCs from five random donors at passages 4-5 cultured in quiescent or proliferative conditions. We isolated 50,000 nuclei and incubated them for 30 minutes with hyperactive Tn5 transposase following the Omni-ATAC protocol[56]. We then amplified the transposed DNA for 8 cycles and inspected for fragment length distribution using an Agilent Bioanalyzer High Sensitivity DNA Chip. This revealed the expected nucleosomal laddering pattern, with subnucleosomal, mononucleosomal, and dinucleosomal fragments enriched at 200, 350, and 550 bp, respectively. We then performed 75 bp paired-end sequencing using Illumina NextSeq 500. We aligned the reads to the human reference genome using Bowtie2[57], removed the mitochondrial DNA reads, retained the uniquely mapped reads, and removed duplicates with SAMTools[58]. After these quality control steps, >95% of the reads mapped to the human genome. We merged the BAM files of individual samples for each culture condition. We called the accessible chromatin region peaks for each of the two merged files using MACS2[59] with parameters -f BAMPE and -q 0.1. Fraction of reads in called peak regions were greater than 0.3. We overlapped the genomic coordinates of SNPs of interest with ATACseq peaks using BEDTools intersect[60].

To evaluate whether eQTL SNPs overlapped with putative transcription factor (TF) binding sites, we overlapped eQTLs located in accessible chromatin regions with sites within TF consensus motifs. We utilized the SNP2TFBS resource of estimated effects of SNPs on predicted TF binding, based on the conformity of motif alleles to the genome[61]. For this analysis, we considered the lead SNPs and their LD proxies ($r^2 \geq 0.8$) found in our eQTL study. TF enrichment values were calculated as the ratio of the observed SNP hits over the expected ones for each TF. We considered enrichment for each TF then using an FDR cutoff of 0.05. TF enrichment was completed separately for each culture condition using the respective eQTL SNPs and ATAC-seq peaks.

Gene silencing, RNA sequencing and proliferation

Since human single-cell ATACseq results from coronary atherosclerosis plaques revealed the SMC specificity of SNHG18 regulatory elements[62], we used human immortalized coronary artery smooth muscle cells (HCASMC) which express SNHG18 similar to aortic SMCs. We transfected HCASMC, which were maintained in M231 medium (Gibco, M231500) supplemented with SMGS (Gibco, S00725), with control (ThermoFisher, 4390846) or SNHG18 (s452763) siRNA using oligofectamine (Invitrogen, 12252011) per manufacturer's standard protocol. To measure the extent of downregulation, we collected the cells after 48 hours and extracted the RNA using QIAGEN RNeasy Plus Mini Kit and performed qPCR for GAPDH and SNHG18. We used the following primer pairs: GAPDH-F: TCGGAGTCAACGGATTTG and GAPDH-R: CAACAATATCCACTTTACCAGAG; SNHG18-F: ATGACTGTGGGCCATGAGTG and SNHG18-R: AAAGCAGCCCTAGGCAATCT. ΔΔCt method was used to calculate the relative gene expression of SNHG18 compared to GAPDH housekeeping gene. We prepared the libraries using the QuantSeq 3′ mRNA-Seq Library Prep Kit FWD for Illumina (Lexogen) according to the manufacturer's instructions. For each sample, we used 250 ng of total RNA for the library preparation, and we sequenced the libraries using a read length of 78 bases (single-end) on an Illumina NextSeq 500 sequencer. We used the nf-core RNA-Seq pipeline[63] to align the reads to the GRCh37/hg19 human genome with the STAR aligner[33] and count the reads in transcripts according to the Ensembl GRCh37 release gene annotations. We identified the differentially expressed genes using DESeq2 package[38] using the default parameters. We performed Gene ontology analysis using the ShinyGO graphical tool for enrichment analysis[64]. Lastly, we performed the proliferation assay in a 96-well plate using the Incucyte S3 Live-Cell Analysis System with the Incucyte Nuclight Rapid Red Dye for nuclear labeling. To monitor cell proliferation, we performed imaging every two hours for four days.

RNAscope in situ hybridization combined with immunohistochemistry

We performed RNAScope™ Double ISH (Advanced Cell Diagnostics, Inc.) following the RNAScope™ Multiplex Fluorescent Reagent Kit v2 User Manual for cultured adherent cells[65]. Briefly, we incubated the slides with hydrogen peroxide for 10 min, treated them with target retrieval reagents for 15 min, and added the hydrophobic barriers around the sections. We applied protease III Reagent for 15 min and later incubated sections with target probes for *ACTA2* (Hs-ACTA2-C1, *GenBank:* NM_001141945.1, target region bases 45 - 1242, Cat No. 311811) and *SNHG18* (Hs-SNHG18-C2, Gen Bank: target region bases: Cat No: 1167101-C2) probes for 2 hours. All target probes consisted of 20 ZZ oligonucleotides obtained from Advanced Cell Diagnostics. Following probe hybridization, sections underwent a series of probe signal amplification steps followed by incubation of fluorescently labeled probes designed to target the specified channel associated with each probe. We counterstained the slides with DAPI and mounted coverslips with FluoromountG (Southern Biotech). We took images using a Zeiss 700 confocal microscope system and we performed the analysis of images using ImageJ software from NIH Image (version 1.34e)[66]. Positive signals were identified as punctate dots, and clusters present around the nucleus and/or cytoplasm.

Supplementary Figures

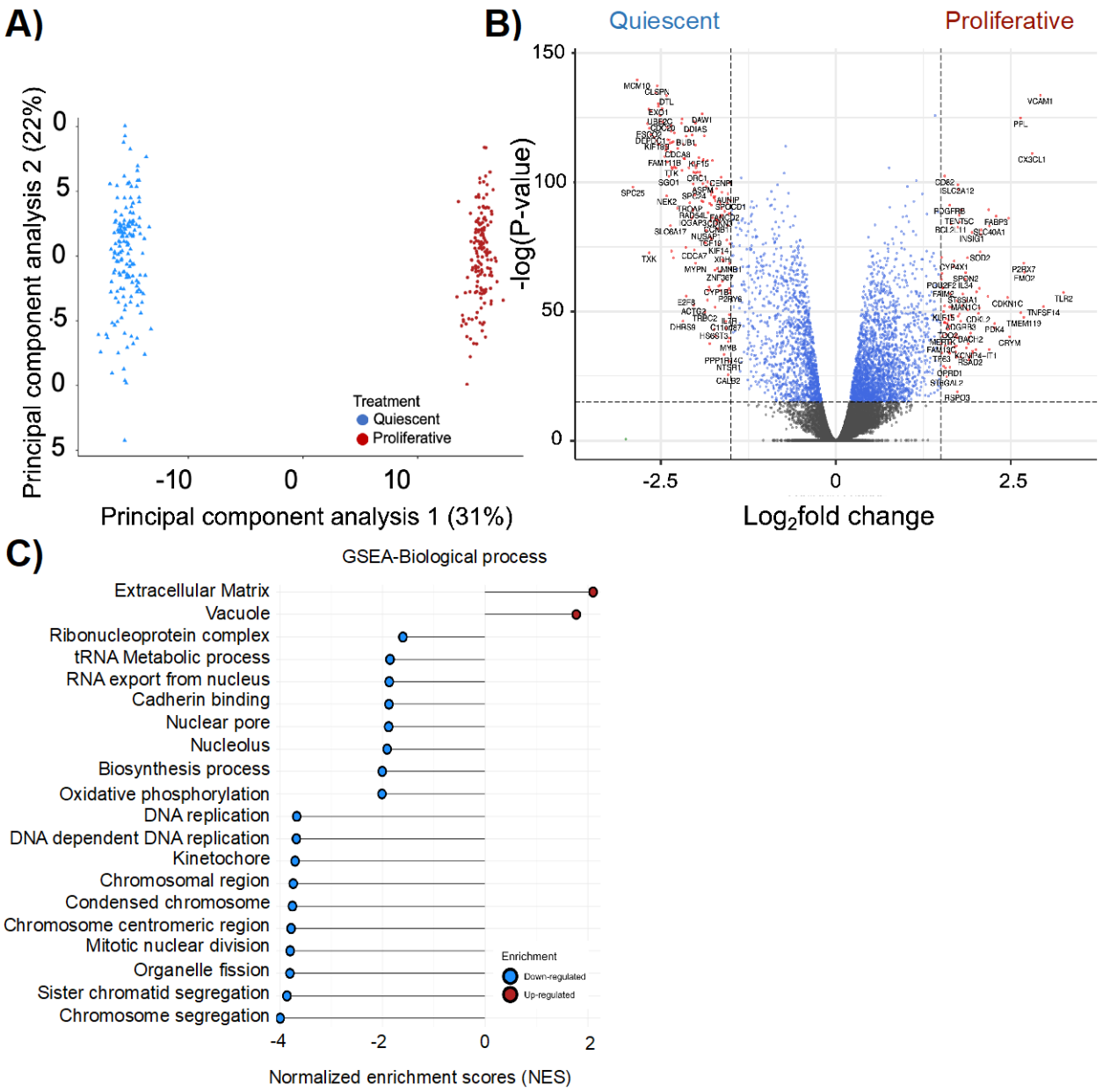

Supplementary Figure 1: Transcriptional profiling of human aortic smooth muscle cells. A) Principal component analysis of gene expression in quiescent and proliferative conditions. **B)** Volcano plot of the expression profiles of genes down and upregulated in SMCs cultured in quiescent and proliferative conditions. The red points represent the differentially expressed genes, gray points represent genes with no difference in their expression. The vertical dashed lines correspond to a 1.5-fold change in expression (up or down), and the horizontal dashed line represents the adjusted P-value (P_{adj}<0.05). **C)** Gene Ontology (GO) pathway analysis of the 2,773 differentially expressed genes, up-regulated (red) and down-regulated (blue) in quiescent and proliferative conditions.

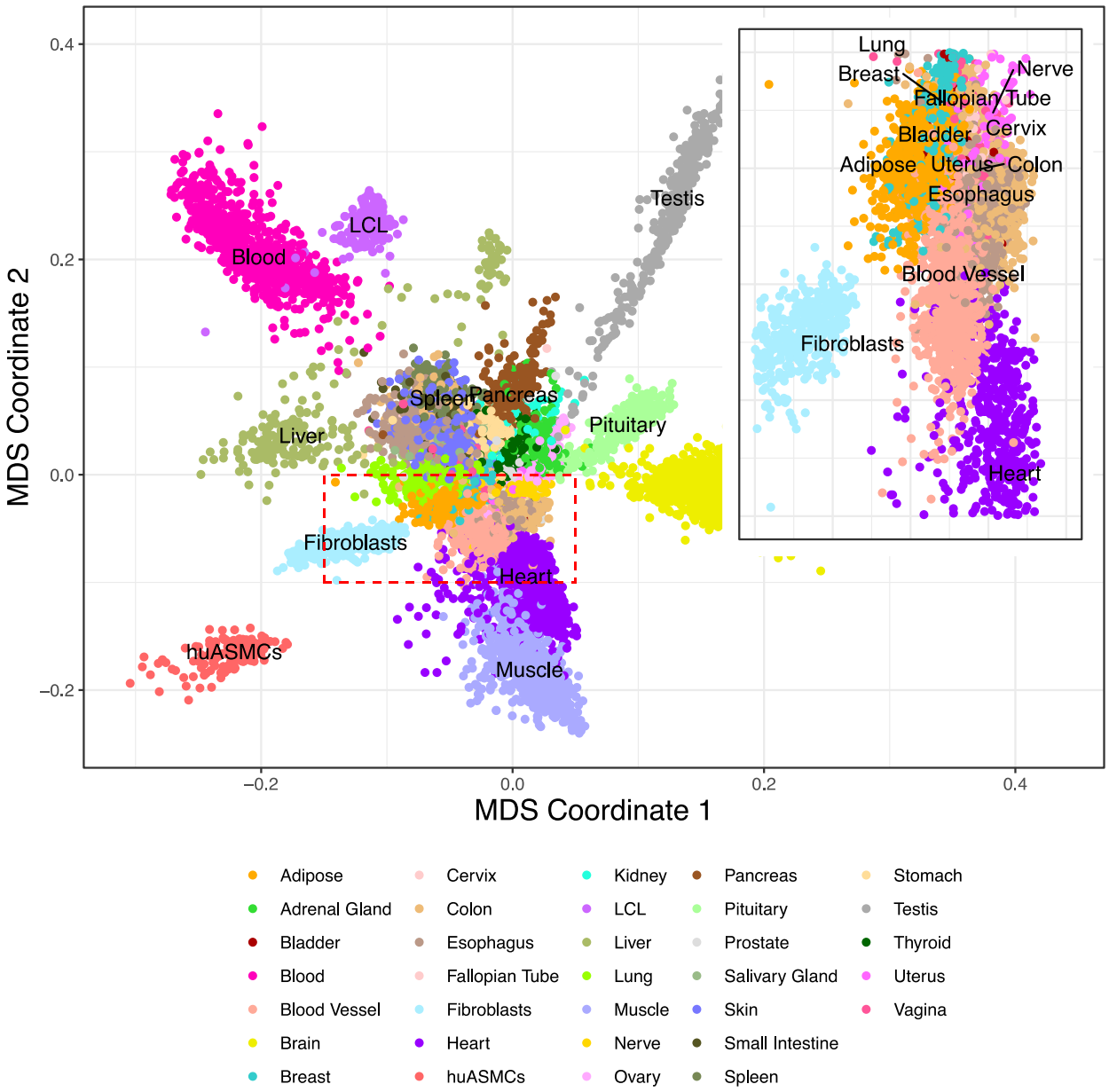

Supplementary Figure 2: Comparison of aortic smooth muscle cell transcriptome with the transcriptomes of tissues and cells profiled in the Genotype-Tissue Expression (GTEx) project. The multidimensional scaling plot of gene expression of SMCs and GTEx tissues and cell types shows a distinct cluster, which neighbors fibroblasts, skeletal muscle, blood vessels and heart (inset).

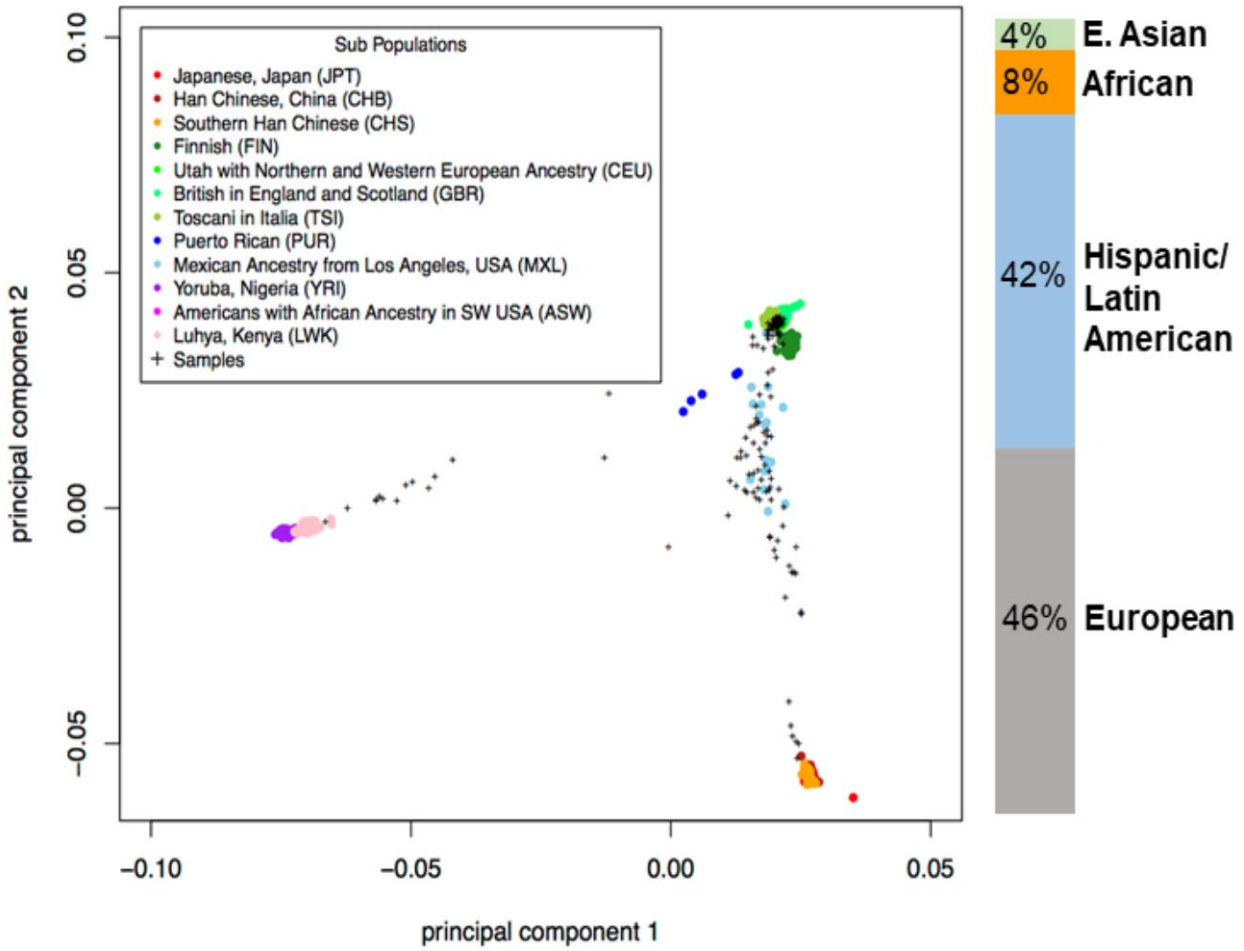

Supplementary Figure 3: Genetic ancestry analysis of SMC donor population. Principal component analysis of the genotypes of the 151 donors in our population and 1000 Genomes populations. The colors indicate different 1000 Genomes reference samples. Donors are represented with "+" and black color.

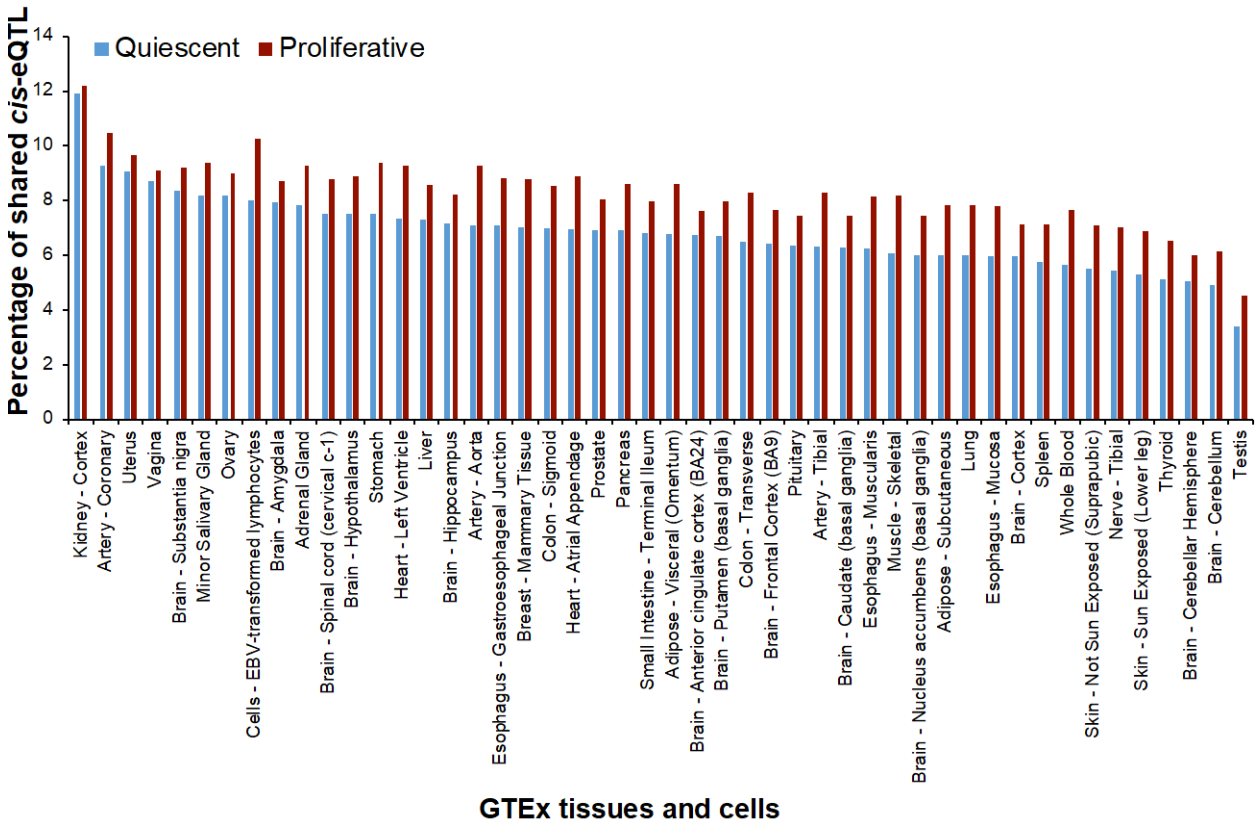

Supplementary Figure 4: Shared *cis*-eQTLs between SMCs and GTEx tissues and cells. The significant SNP-gene pairs for each SMC *cis*-eQTL (FDR q-value <0.05) was queried for their presence among the *cis*-eQTL signals in GTEx v8 (FDR q-value <0.05)[49]. Percentage of the shared *cis*-eQTLs was calculated based on the total number of *cis*-eQTL in each GTEx tissue separately since the number of donors for each tissue is different.

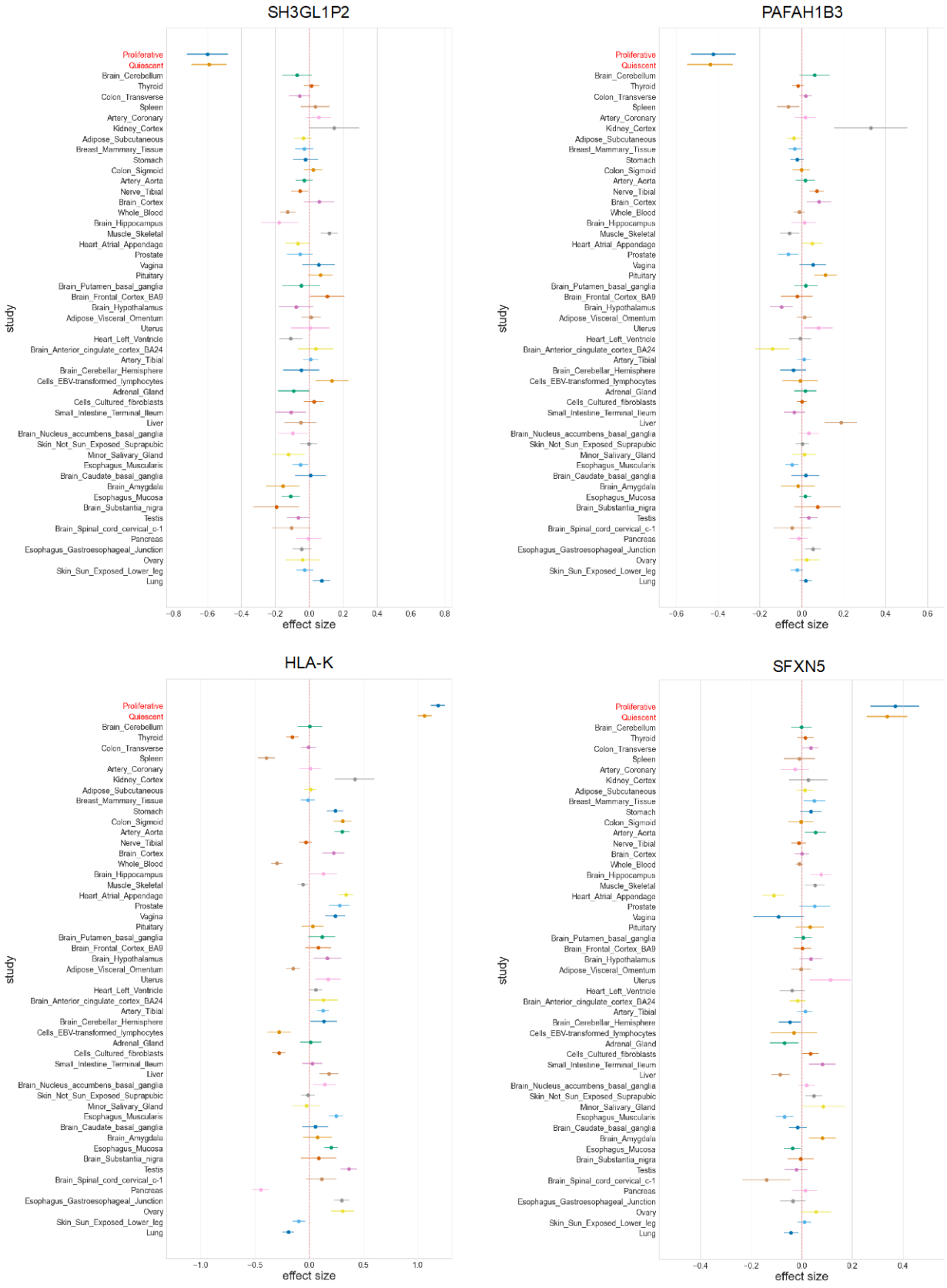
SH3GL1P2
PAFAH1B3
HLA-K
SFXN5
study
effect size
Proliferative
Quiescent
Brain_Cerebellum
Thyroid
Colon_Transverse
Spleen
Artery_Coronary
Kidney_Cortex
Adipose_Subcutaneous
Breast_Mammary_Tissue
Stomach
Colon_Sigmoid
Artery_Aorta
Nerve_Tibial
Brain_Cortex
Whole_Blood
Brain_Hippocampus
Muscle_Skeletal
Heart_Atrial_Appendage
Prostate
Vagina
Pituitary
Brain_Putamen_basal_ganglia
Brain_Frontal_Cortex_BA9
Brain_Hypothalamus
Adipose_Visceral_Omentum
Uterus
Heart_Left_Ventricle
Brain_Anterior_cingulate_cortex_BA24
Artery_Tibial
Brain_Cerebellar_Hemisphere
Cells_EBV-transformed_lymphocytes
Adrenal_Gland
Cells_Cultured_fibroblasts
Small_Intestine_Terminal_Ileum
Liver
Brain_Nucleus_accumbens_basal_ganglia
Skin_Not_Sun_Exposed_Suprapubic
Minor_Salivary_Gland
Esophagus_Muscularis
Brain_Caudate_basal_ganglia
Brain_Amygdala
Esophagus_Mucosa
Brain_Substantia_nigra
Testis
Brain_Spinal_cord_cervical_c-1
Pancreas
Esophagus_Gastroesophageal_Junction
Ovary
Skin_Sun_Exposed_Lower_leg
Lung


INTS11
Proliferative
Quiescent
Brain_Cerebellum
Thyroid
Colon_Transverse
Spleen
Artery_Coronary
Kidney_Cortex
Adipose_Subcutaneous
Breast_Mammary_Tissue
Stomach
Colon_Sigmoid
Artery_Aorta
Nerve_Tibial
Brain_Cortex
Whole_Blood
Brain_Hippocampus
Muscle_Skeletal
Heart_Atrial_Appendage
Prostate
Vagina
Pituitary
Brain_Putamen_basal_ganglia
Brain_Frontal_Cortex_BA9
Brain_Hypothalamus
Adipose_Visceral_Omentum
Uterus
Heart_Left_Ventricle
Brain_Anterior_cingulate_cortex_BA24
Artery_Tibial
Brain_Cerebellar_Hemisphere
Cells_EBV-transformed_lymphocytes
Adrenal_Gland
Cells_Cultured_fibroblasts
Small_Intestine_Terminal_Ileum
Liver
Brain_Nucleus_accumbens_basal_ganglia
Skin_Not_Sun_Exposed_Suprapubic
Minor_Salivary_Gland
Esophagus_Muscularis
Brain_Caudate_basal_ganglia
Brain_Amygdala
Esophagus_Mucosa
Brain_Substantia_nigra
Testis
Brain_Spinal_cord_cervical_c-1
Pancreas
Esophagus_Gastroesophageal_Junction
Ovary
Skin_Sun_Exposed_Lower_leg
Lung
study
−0.3
−0.2
−0.1
0.0
0.1
0.2
0.3
effect size

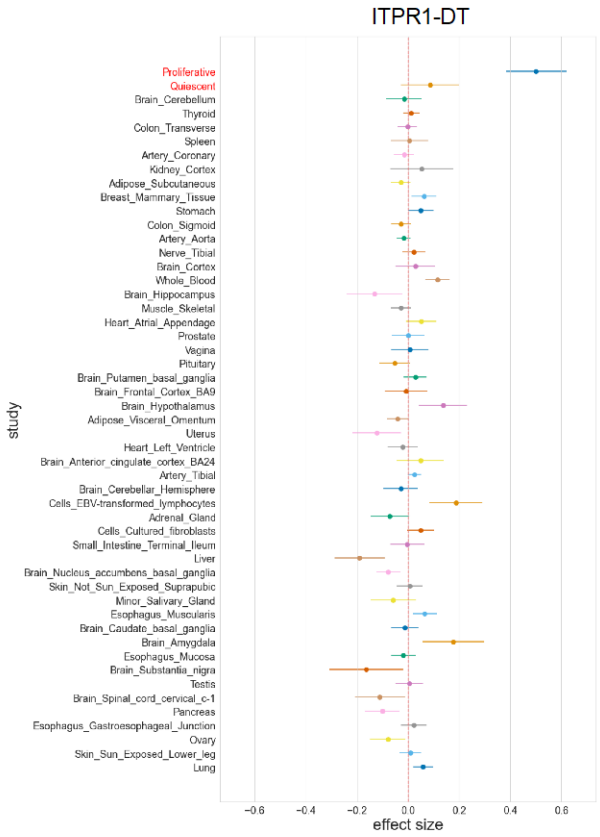
ITPR1-DT
Proliferative
Quiescent
Brain_Cerebellum
Thyroid
Colon_Transverse
Spleen
Artery_Coronary
Kidney_Cortex
Adipose_Subcutaneous
Breast_Mammary_Tissue
Stomach
Colon_Sigmoid
Artery_Aorta
Nerve_Tibial
Brain_Cortex
Whole_Blood
Brain_Hippocampus
Muscle_Skeletal
Heart_Atrial_Appendage
Prostate
Vagina
Pituitary
Brain_Putamen_basal_ganglia
Brain_Frontal_Cortex_BA9
Brain_Hypothalamus
Adipose_Visceral_Omentum
Uterus
Heart_Left_Ventricle
Brain_Anterior_cingulate_cortex_BA24
Artery_Tibial
Brain_Cerebellar_Hemisphere
Cells_EBV-transformed_lymphocytes
Adrenal_Gland
Cells_Cultured_fibroblasts
Small_Intestine_Terminal_Ileum
Liver
Brain_Nucleus_accumbens_basal_ganglia
Skin_Not_Sun_Exposed_Suprapubic
Minor_Salivary_Gland
Esophagus_Muscularis
Brain_Caudate_basal_ganglia
Brain_Amygdala
Esophagus_Mucosa
Brain_Substantia_nigra
Testis
Brain_Spinal_cord_cervical_c-1
Pancreas
Esophagus_Gastroesophageal_Junction
Ovary
Skin_Sun_Exposed_Lower_leg
Lung
study
−0.6
−0.4
−0.2
0.0
0.2
0.4
0.6
effect size

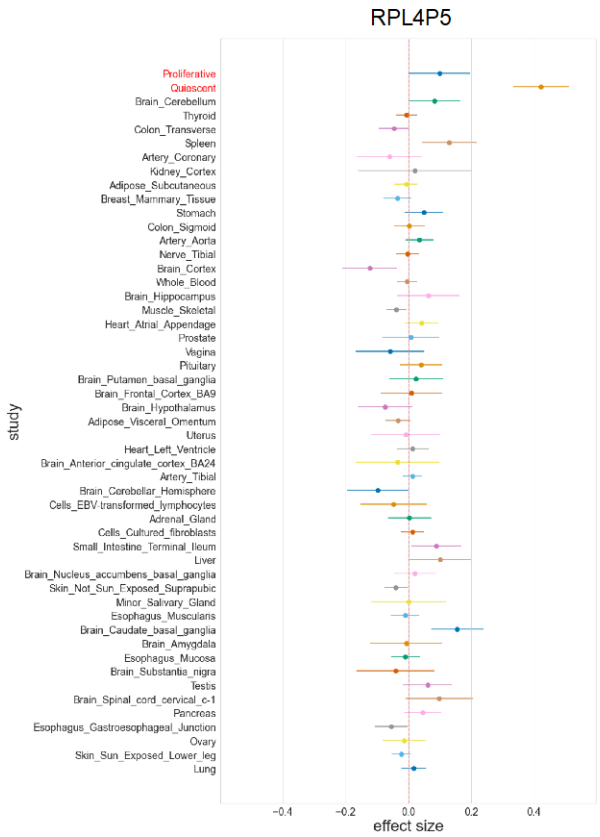
RPL4P5
Proliferative
Quiescent
Brain_Cerebellum
Thyroid
Colon_Transverse
Spleen
Artery_Coronary
Kidney_Cortex
Adipose_Subcutaneous
Breast_Mammary_Tissue
Stomach
Colon_Sigmoid
Artery_Aorta
Nerve_Tibial
Brain_Cortex
Whole_Blood
Brain_Hippocampus
Muscle_Skeletal
Heart_Atrial_Appendage
Prostate
Vagina
Pituitary
Brain_Putamen_basal_ganglia
Brain_Frontal_Cortex_BA9
Brain_Hypothalamus
Adipose_Visceral_Omentum
Uterus
Heart_Left_Ventricle
Brain_Anterior_cingulate_cortex_BA24
Artery_Tibial
Brain_Cerebellar_Hemisphere
Cells_EBV-transformed_lymphocytes
Adrenal_Gland
Cells_Cultured_fibroblasts
Small_Intestine_Terminal_Ileum
Liver
Brain_Nucleus_accumbens_basal_ganglia
Skin_Not_Sun_Exposed_Suprapubic
Minor_Salivary_Gland
Esophagus_Muscularis
Brain_Caudate_basal_ganglia
Brain_Amygdala
Esophagus_Mucosa
Brain_Substantia_nigra
Testis
Brain_Spinal_cord_cervical_c-1
Pancreas
Esophagus_Gastroesophageal_Junction
Ovary
Skin_Sun_Exposed_Lower_leg
Lung
study
−0.4
−0.2
0.0
0.2
0.4
effect size

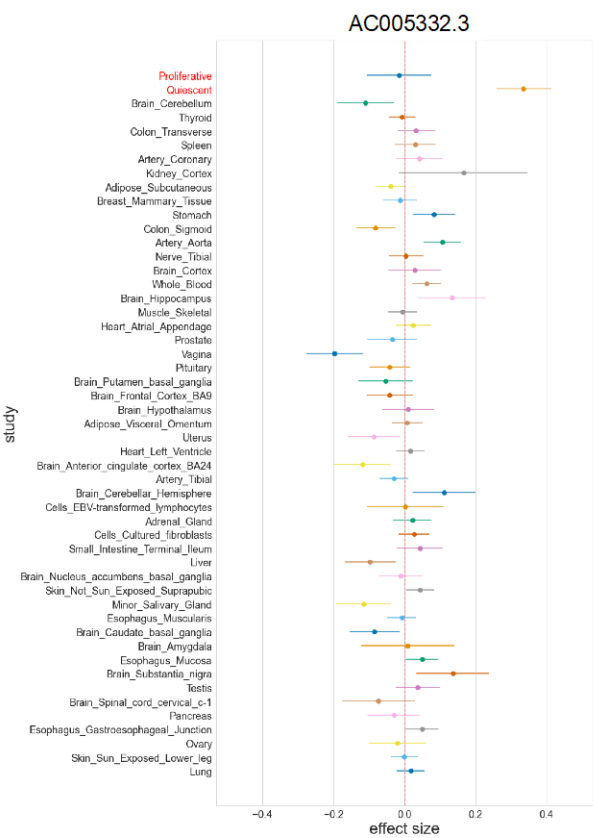
AC005332.3
Proliferative
Quiescent
Brain_Cerebellum
Thyroid
Colon_Transverse
Spleen
Artery_Coronary
Kidney_Cortex
Adipose_Subcutaneous
Breast_Mammary_Tissue
Stomach
Colon_Sigmoid
Artery_Aorta
Nerve_Tibial
Brain_Cortex
Whole_Blood
Brain_Hippocampus
Muscle_Skeletal
Heart_Atrial_Appendage
Prostate
Vagina
Pituitary
Brain_Putamen_basal_ganglia
Brain_Frontal_Cortex_BA9
Brain_Hypothalamus
Adipose_Visceral_Omentum
Uterus
Heart_Left_Ventricle
Brain_Anterior_cingulate_cortex_BA24
Artery_Tibial
Brain_Cerebellar_Hemisphere
Cells_EBV-transformed_lymphocytes
Adrenal_Gland
Cells_Cultured_fibroblasts
Small_Intestine_Terminal_Ileum
Liver
Brain_Nucleus_accumbens_basal_ganglia
Skin_Not_Sun_Exposed_Suprapubic
Minor_Salivary_Gland
Esophagus_Muscularis
Brain_Caudate_basal_ganglia
Brain_Amygdala
Esophagus_Mucosa
Brain_Substantia_nigra
Testis
Brain_Spinal_cord_cervical_c-1
Pancreas
Esophagus_Gastroesophageal_Junction
Ovary
Skin_Sun_Exposed_Lower_leg
Lung
study
−0.4
−0.2
0.0
0.2
0.4
effect size


PMAIP1
study
Proliferative
Quiescent
Brain_Cerebellum
Thyroid
Colon_Transverse
Spleen
Artery_Coronary
Kidney_Cortex
Adipose_Subcutaneous
Breast_Mammary_Tissue
Stomach
Colon_Sigmoid
Artery_Aorta
Nerve_Tibial
Brain_Cortex
Whole_Blood
Brain_Hippocampus
Muscle_Skeletal
Heart_Atrial_Appendage
Prostate
Vagina
Pituitary
Brain_Putamen_basal_ganglia
Brain_Frontal_Cortex_BA9
Brain_Hypothalamus
Adipose_Visceral_Omentum
Uterus
Heart_Left_Ventricle
Brain_Anterior_cingulate_cortex_BA24
Artery_Tibial
Brain_Cerebellar_Hemisphere
Cells_EBV-transformed_lymphocytes
Adrenal_Gland
Cells_Cultured_fibroblasts
Small_Intestine_Terminal_Ileum
Liver
Brain_Nucleus_accumbens_basal_ganglia
Skin_Not_Sun_Exposed_Suprapubic
Minor_Salivary_Gland
Esophagus_Muscularis
Brain_Caudate_basal_ganglia
Brain_Amygdala
Esophagus_Mucosa
Brain_Substantia_nigra
Testis
Brain_Spinal_cord_cervical_c-1
Pancreas
Esophagus_Gastroesophageal_Junction
Ovary
Skin_Sun_Exposed_Lower_leg
Lung
−1.0
−0.5
0.0
0.5
1.0
effect size

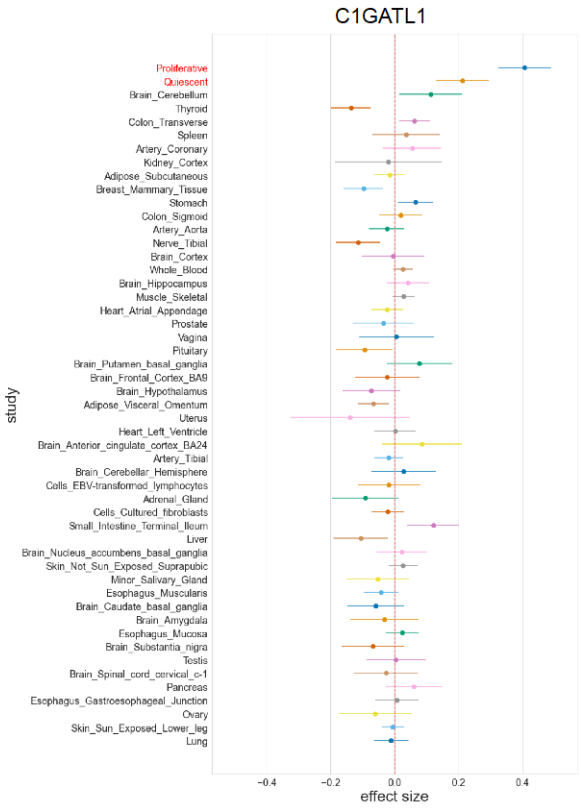
C1GATL1
study
Proliferative
Quiescent
Brain_Cerebellum
Thyroid
Colon_Transverse
Spleen
Artery_Coronary
Kidney_Cortex
Adipose_Subcutaneous
Breast_Mammary_Tissue
Stomach
Colon_Sigmoid
Artery_Aorta
Nerve_Tibial
Brain_Cortex
Whole_Blood
Brain_Hippocampus
Muscle_Skeletal
Heart_Atrial_Appendage
Prostate
Vagina
Pituitary
Brain_Putamen_basal_ganglia
Brain_Frontal_Cortex_BA9
Brain_Hypothalamus
Adipose_Visceral_Omentum
Uterus
Heart_Left_Ventricle
Brain_Anterior_cingulate_cortex_BA24
Artery_Tibial
Brain_Cerebellar_Hemisphere
Cells_EBV-transformed_lymphocytes
Adrenal_Gland
Cells_Cultured_fibroblasts
Small_Intestine_Terminal_Ileum
Liver
Brain_Nucleus_accumbens_basal_ganglia
Skin_Not_Sun_Exposed_Suprapubic
Minor_Salivary_Gland
Esophagus_Muscularis
Brain_Caudate_basal_ganglia
Brain_Amygdala
Esophagus_Mucosa
Brain_Substantia_nigra
Testis
Brain_Spinal_cord_cervical_c-1
Pancreas
Esophagus_Gastroesophageal_Junction
Ovary
Skin_Sun_Exposed_Lower_leg
Lung
−0.4
−0.2
0.0
0.2
0.4
effect size


RAB3IP
study
Proliferative
Quiescent
Brain_Cerebellum
Thyroid
Colon_Transverse
Spleen
Artery_Coronary
Kidney_Cortex
Adipose_Subcutaneous
Breast_Mammary_Tissue
Stomach
Colon_Sigmoid
Artery_Aorta
Nerve_Tibial
Brain_Cortex
Whole_Blood
Brain_Hippocampus
Muscle_Skeletal
Heart_Atrial_Appendage
Prostate
Vagina
Pituitary
Brain_Putamen_basal_ganglia
Brain_Frontal_Cortex_BA9
Brain_Hypothalamus
Adipose_Visceral_Omentum
Uterus
Heart_Left_Ventricle
Brain_Anterior_cingulate_cortex_BA24
Artery_Tibial
Brain_Cerebellar_Hemisphere
Cells_EBV-transformed_lymphocytes
Adrenal_Gland
Cells_Cultured_fibroblasts
Small_Intestine_Terminal_Ileum
Liver
Brain_Nucleus_accumbens_basal_ganglia
Skin_Not_Sun_Exposed_Suprapubic
Minor_Salivary_Gland
Esophagus_Muscularis
Brain_Caudate_basal_ganglia
Brain_Amygdala
Esophagus_Mucosa
Brain_Substantia_nigra
Testis
Brain_Spinal_cord_cervical_c-1
Pancreas
Esophagus_Gastroesophageal_Junction
Ovary
Skin_Sun_Exposed_Lower_leg
Lung
−0.75
−0.50
−0.25
0.00
0.25
0.50
0.75
effect size

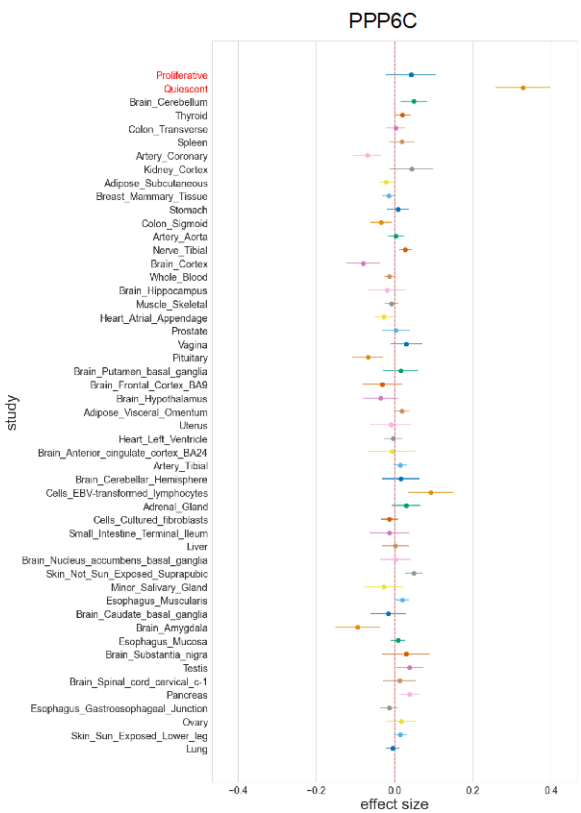
PPP6C
study
Proliferative
Quiescent
Brain_Cerebellum
Thyroid
Colon_Transverse
Spleen
Artery_Coronary
Kidney_Cortex
Adipose_Subcutaneous
Breast_Mammary_Tissue
Stomach
Colon_Sigmoid
Artery_Aorta
Nerve_Tibial
Brain_Cortex
Whole_Blood
Brain_Hippocampus
Muscle_Skeletal
Heart_Atrial_Appendage
Prostate
Vagina
Pituitary
Brain_Putamen_basal_ganglia
Brain_Frontal_Cortex_BA9
Brain_Hypothalamus
Adipose_Visceral_Omentum
Uterus
Heart_Left_Ventricle
Brain_Anterior_cingulate_cortex_BA24
Artery_Tibial
Brain_Cerebellar_Hemisphere
Cells_EBV-transformed_lymphocytes
Adrenal_Gland
Cells_Cultured_fibroblasts
Small_Intestine_Terminal_Ileum
Liver
Brain_Nucleus_accumbens_basal_ganglia
Skin_Not_Sun_Exposed_Suprapubic
Minor_Salivary_Gland
Esophagus_Muscularis
Brain_Caudate_basal_ganglia
Brain_Amygdala
Esophagus_Mucosa
Brain_Substantia_nigra
Testis
Brain_Spinal_cord_cervical_c-1
Pancreas
Esophagus_Gastroesophageal_Junction
Ovary
Skin_Sun_Exposed_Lower_leg
Lung
−0.4
−0.2
0.0
0.2
0.4
effect size

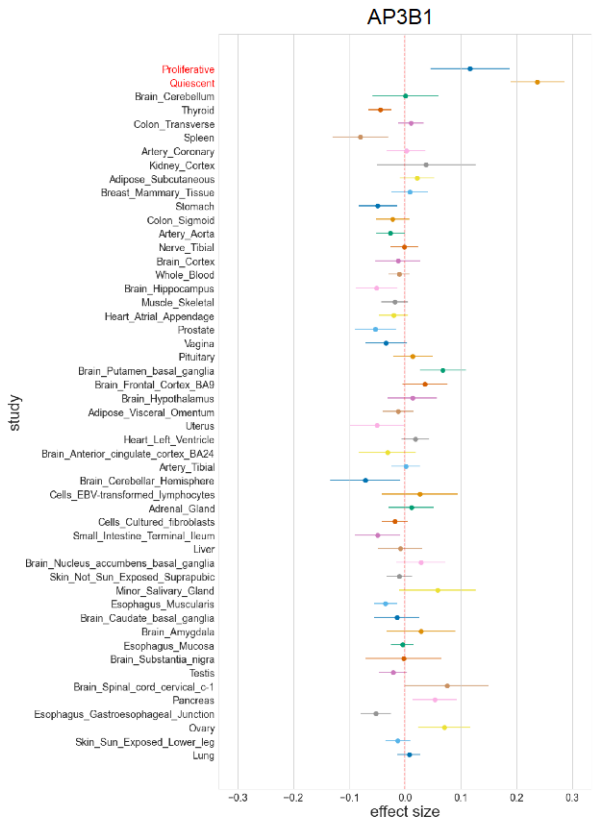
AP3B1
Proliferative
Quiescent
Brain_Cerebellum
Thyroid
Colon_Transverse
Spleen
Artery_Coronary
Kidney_Cortex
Adipose_Subcutaneous
Breast_Mammary_Tissue
Stomach
Colon_Sigmoid
Artery_Aorta
Nerve_Tibial
Brain_Cortex
Whole_Blood
Brain_Hippocampus
Muscle_Skeletal
Heart_Atrial_Appendage
Prostate
Vagina
Pituitary
Brain_Putamen_basal_ganglia
Brain_Frontal_Cortex_BA9
Brain_Hypothalamus
Adipose_Visceral_Omentum
Uterus
Heart_Left_Ventricle
Brain_Anterior_cingulate_cortex_BA24
Artery_Tibial
Brain_Cerebellar_Hemisphere
Cells_EBV-transformed_lymphocytes
Adrenal_Gland
Cells_Cultured_fibroblasts
Small_Intestine_Terminal_Ileum
Liver
Brain_Nucleus_accumbens_basal_ganglia
Skin_Not_Sun_Exposed_Suprapubic
Minor_Salivary_Gland
Esophagus_Muscularis
Brain_Caudate_basal_ganglia
Brain_Amygdala
Esophagus_Mucosa
Brain_Substantia_nigra
Testis
Brain_Spinal_cord_cervical_c-1
Pancreas
Esophagus_Gastroesophageal_Junction
Ovary
Skin_Sun_Exposed_Lower_leg
Lung
study
−0.3
−0.2
−0.1
0.0
0.1
0.2
0.3
effect size

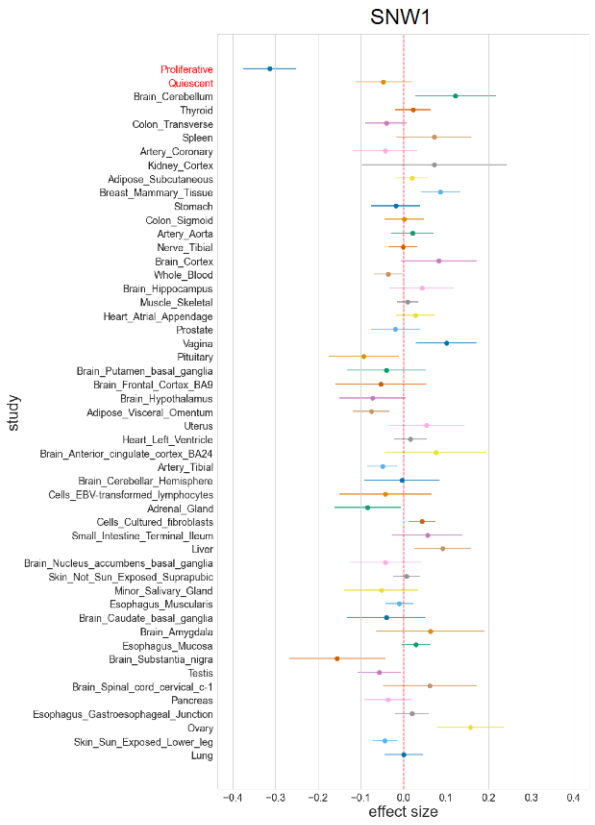
SNW1
Proliferative
Quiescent
Brain_Cerebellum
Thyroid
Colon_Transverse
Spleen
Artery_Coronary
Kidney_Cortex
Adipose_Subcutaneous
Breast_Mammary_Tissue
Stomach
Colon_Sigmoid
Artery_Aorta
Nerve_Tibial
Brain_Cortex
Whole_Blood
Brain_Hippocampus
Muscle_Skeletal
Heart_Atrial_Appendage
Prostate
Vagina
Pituitary
Brain_Putamen_basal_ganglia
Brain_Frontal_Cortex_BA9
Brain_Hypothalamus
Adipose_Visceral_Omentum
Uterus
Heart_Left_Ventricle
Brain_Anterior_cingulate_cortex_BA24
Artery_Tibial
Brain_Cerebellar_Hemisphere
Cells_EBV-transformed_lymphocytes
Adrenal_Gland
Cells_Cultured_fibroblasts
Small_Intestine_Terminal_Ileum
Liver
Brain_Nucleus_accumbens_basal_ganglia
Skin_Not_Sun_Exposed_Suprapubic
Minor_Salivary_Gland
Esophagus_Muscularis
Brain_Caudate_basal_ganglia
Brain_Amygdala
Esophagus_Mucosa
Brain_Substantia_nigra
Testis
Brain_Spinal_cord_cervical_c-1
Pancreas
Esophagus_Gastroesophageal_Junction
Ovary
Skin_Sun_Exposed_Lower_leg
Lung
study
−0.4
−0.3
−0.2
−0.1
0.0
0.1
0.2
0.3
0.4
effect size

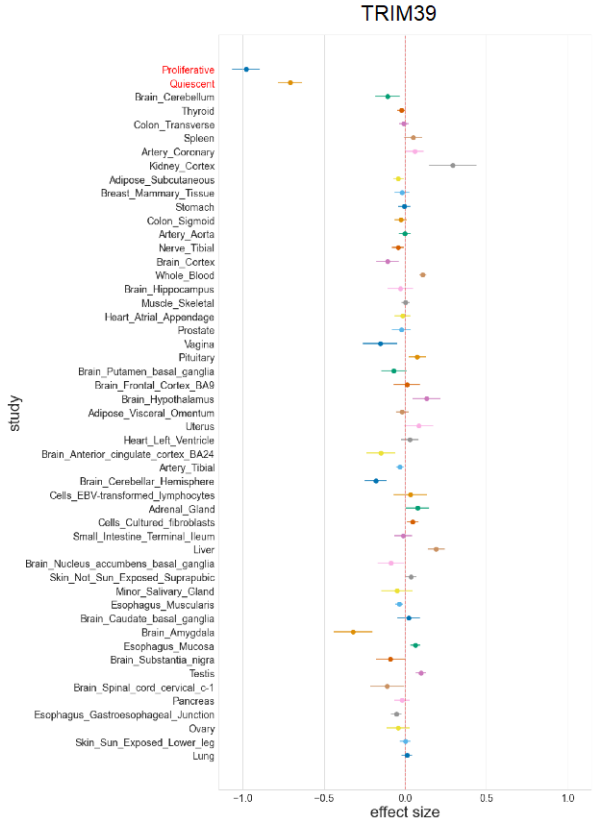
TRIM39
Proliferative
Quiescent
Brain_Cerebellum
Thyroid
Colon_Transverse
Spleen
Artery_Coronary
Kidney_Cortex
Adipose_Subcutaneous
Breast_Mammary_Tissue
Stomach
Colon_Sigmoid
Artery_Aorta
Nerve_Tibial
Brain_Cortex
Whole_Blood
Brain_Hippocampus
Muscle_Skeletal
Heart_Atrial_Appendage
Prostate
Vagina
Pituitary
Brain_Putamen_basal_ganglia
Brain_Frontal_Cortex_BA9
Brain_Hypothalamus
Adipose_Visceral_Omentum
Uterus
Heart_Left_Ventricle
Brain_Anterior_cingulate_cortex_BA24
Artery_Tibial
Brain_Cerebellar_Hemisphere
Cells_EBV-transformed_lymphocytes
Adrenal_Gland
Cells_Cultured_fibroblasts
Small_Intestine_Terminal_Ileum
Liver
Brain_Nucleus_accumbens_basal_ganglia
Skin_Not_Sun_Exposed_Suprapubic
Minor_Salivary_Gland
Esophagus_Muscularis
Brain_Caudate_basal_ganglia
Brain_Amygdala
Esophagus_Mucosa
Brain_Substantia_nigra
Testis
Brain_Spinal_cord_cervical_c-1
Pancreas
Esophagus_Gastroesophageal_Junction
Ovary
Skin_Sun_Exposed_Lower_leg
Lung
study
−1.0
−0.5
0.0
0.5
1.0
effect size


MIER2
Proliferative
Quiescent
Brain_Cerebellum
Thyroid
Colon_Transverse
Spleen
Artery_Coronary
Kidney_Cortex
Adipose_Subcutaneous
Breast_Mammary_Tissue
Stomach
Colon_Sigmoid
Artery_Aorta
Nerve_Tibial
Brain_Cortex
Whole_Blood
Brain_Hippocampus
Muscle_Skeletal
Heart_Atrial_Appendage
Prostate
Vagina
Pituitary
Brain_Putamen_basal_ganglia
Brain_Frontal_Cortex_BA9
Brain_Hypothalamus
Adipose_Visceral_Omentum
Uterus
Heart_Left_Ventricle
Brain_Anterior_cingulate_cortex_BA24
Artery_Tibial
Brain_Cerebellar_Hemisphere
Cells_EBV-transformed_lymphocytes
Adrenal_Gland
Cells_Cultured_fibroblasts
Small_Intestine_Terminal_Ileum
Liver
Brain_Nucleus_accumbens_basal_ganglia
Skin_Not_Sun_Exposed_Suprapubic
Minor_Salivary_Gland
Esophagus_Muscularis
Brain_Caudate_basal_ganglia
Brain_Amygdala
Esophagus_Mucosa
Brain_Substantia_nigra
Testis
Brain_Spinal_cord_cervical_c-1
Pancreas
Esophagus_Gastroesophageal_Junction
Ovary
Skin_Sun_Exposed_Lower_leg
Lung
study
−0.4
−0.3
−0.2
−0.1
0.0
0.1
0.2
0.3
0.4
effect size

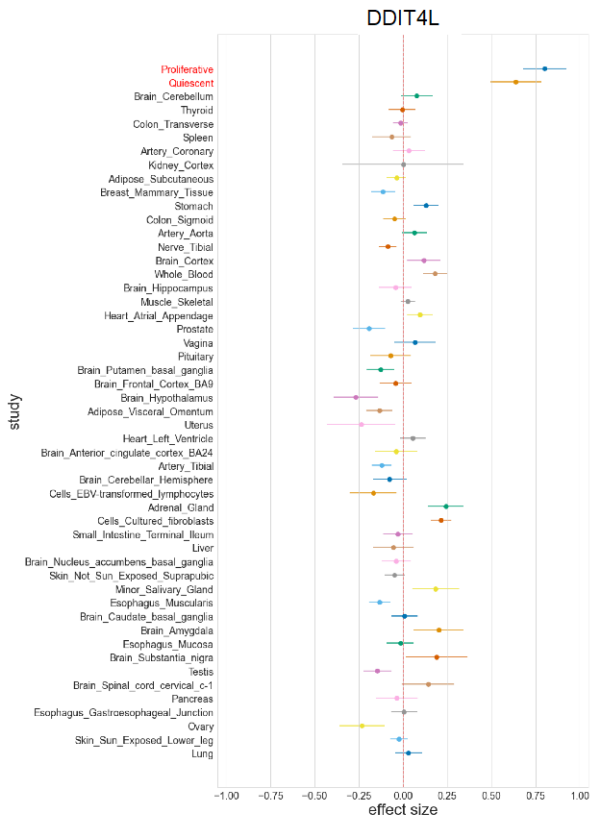
DDIT4L
Proliferative
Quiescent
Brain_Cerebellum
Thyroid
Colon_Transverse
Spleen
Artery_Coronary
Kidney_Cortex
Adipose_Subcutaneous
Breast_Mammary_Tissue
Stomach
Colon_Sigmoid
Artery_Aorta
Nerve_Tibial
Brain_Cortex
Whole_Blood
Brain_Hippocampus
Muscle_Skeletal
Heart_Atrial_Appendage
Prostate
Vagina
Pituitary
Brain_Putamen_basal_ganglia
Brain_Frontal_Cortex_BA9
Brain_Hypothalamus
Adipose_Visceral_Omentum
Uterus
Heart_Left_Ventricle
Brain_Anterior_cingulate_cortex_BA24
Artery_Tibial
Brain_Cerebellar_Hemisphere
Cells_EBV-transformed_lymphocytes
Adrenal_Gland
Cells_Cultured_fibroblasts
Small_Intestine_Terminal_Ileum
Liver
Brain_Nucleus_accumbens_basal_ganglia
Skin_Not_Sun_Exposed_Suprapubic
Minor_Salivary_Gland
Esophagus_Muscularis
Brain_Caudate_basal_ganglia
Brain_Amygdala
Esophagus_Mucosa
Brain_Substantia_nigra
Testis
Brain_Spinal_cord_cervical_c-1
Pancreas
Esophagus_Gastroesophageal_Junction
Ovary
Skin_Sun_Exposed_Lower_leg
Lung
study
−1.00 −0.75 −0.50 −0.25 0.00 0.25 0.50 0.75 1.00
effect size

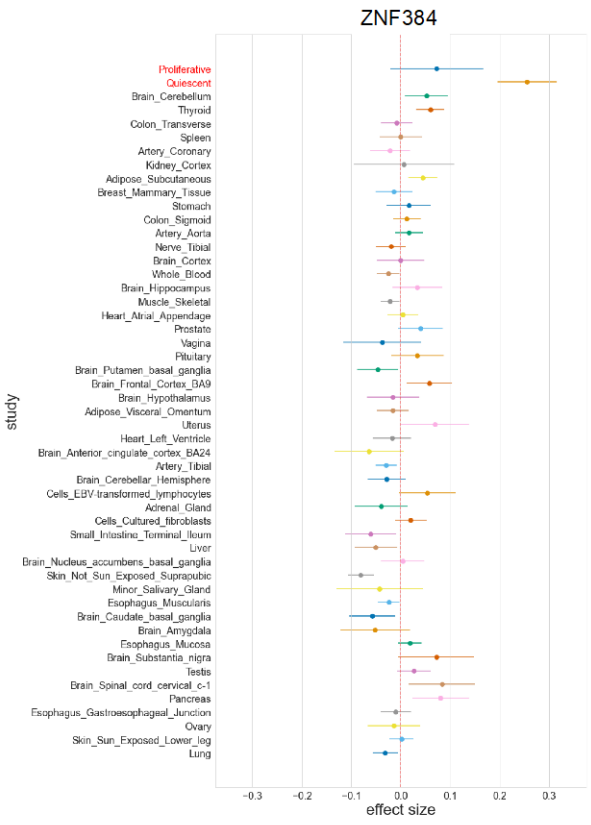
ZNF384
Proliferative
Quiescent
Brain_Cerebellum
Thyroid
Colon_Transverse
Spleen
Artery_Coronary
Kidney_Cortex
Adipose_Subcutaneous
Breast_Mammary_Tissue
Stomach
Colon_Sigmoid
Artery_Aorta
Nerve_Tibial
Brain_Cortex
Whole_Blood
Brain_Hippocampus
Muscle_Skeletal
Heart_Atrial_Appendage
Prostate
Vagina
Pituitary
Brain_Putamen_basal_ganglia
Brain_Frontal_Cortex_BA9
Brain_Hypothalamus
Adipose_Visceral_Omentum
Uterus
Heart_Left_Ventricle
Brain_Anterior_cingulate_cortex_BA24
Artery_Tibial
Brain_Cerebellar_Hemisphere
Cells_EBV-transformed_lymphocytes
Adrenal_Gland
Cells_Cultured_fibroblasts
Small_Intestine_Terminal_Ileum
Liver
Brain_Nucleus_accumbens_basal_ganglia
Skin_Not_Sun_Exposed_Suprapubic
Minor_Salivary_Gland
Esophagus_Muscularis
Brain_Caudate_basal_ganglia
Brain_Amygdala
Esophagus_Mucosa
Brain_Substantia_nigra
Testis
Brain_Spinal_cord_cervical_c-1
Pancreas
Esophagus_Gastroesophageal_Junction
Ovary
Skin_Sun_Exposed_Lower_leg
Lung
study
−0.3 −0.2 −0.1 0.0 0.1 0.2 0.3
effect size


LTO1
Proliferative
Quiescent
Brain_Cerebellum
Thyroid
Colon_Transverse
Spleen
Artery_Coronary
Kidney_Cortex
Adipose_Subcutaneous
Breast_Mammary_Tissue
Stomach
Colon_Sigmoid
Artery_Aorta
Nerve_Tibial
Brain_Cortex
Whole_Blood
Brain_Hippocampus
Muscle_Skeletal
Heart_Atrial_Appendage
Prostate
Vagina
Pituitary
Brain_Putamen_basal_ganglia
Brain_Frontal_Cortex_BA9
Brain_Hypothalamus
Adipose_Visceral_Omentum
Uterus
Heart_Left_Ventricle
Brain_Anterior_cingulate_cortex_BA24
Artery_Tibial
Brain_Cerebellar_Hemisphere
Cells_EBV-transformed_lymphocytes
Adrenal_Gland
Cells_Cultured_fibroblasts
Small_Intestine_Terminal_Ileum
Liver
Brain_Nucleus_accumbens_basal_ganglia
Skin_Not_Sun_Exposed_Suprapubic
Minor_Salivary_Gland
Esophagus_Muscularis
Brain_Caudate_basal_ganglia
Brain_Amygdala
Esophagus_Mucosa
Brain_Substantia_nigra
Testis
Brain_Spinal_cord_cervical_c-1
Pancreas
Esophagus_Gastroesophageal_Junction
Ovary
Skin_Sun_Exposed_Lower_leg
Lung
study
−0.4 −0.2 0.0 0.2 0.4
effect size

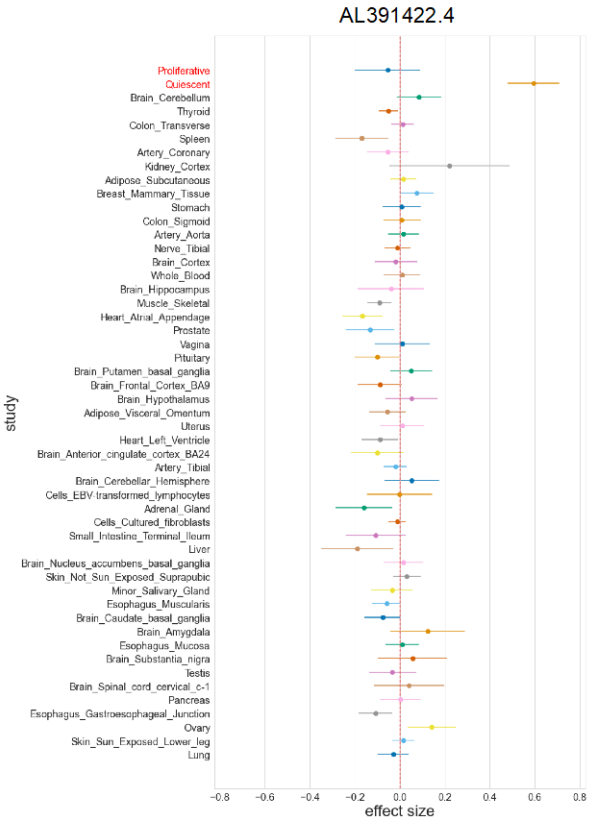
AL391422.4
Proliferative
Quiescent
Brain_Cerebellum
Thyroid
Colon_Transverse
Spleen
Artery_Coronary
Kidney_Cortex
Adipose_Subcutaneous
Breast_Mammary_Tissue
Stomach
Colon_Sigmoid
Artery_Aorta
Nerve_Tibial
Brain_Cortex
Whole_Blood
Brain_Hippocampus
Muscle_Skeletal
Heart_Atrial_Appendage
Prostate
Vagina
Pituitary
Brain_Putamen_basal_ganglia
Brain_Frontal_Cortex_BA9
Brain_Hypothalamus
Adipose_Visceral_Omentum
Uterus
Heart_Left_Ventricle
Brain_Anterior_cingulate_cortex_BA24
Artery_Tibial
Brain_Cerebellar_Hemisphere
Cells_EBV-transformed_lymphocytes
Adrenal_Gland
Cells_Cultured_fibroblasts
Small_Intestine_Terminal_Ileum
Liver
Brain_Nucleus_accumbens_basal_ganglia
Skin_Not_Sun_Exposed_Suprapubic
Minor_Salivary_Gland
Esophagus_Muscularis
Brain_Caudate_basal_ganglia
Brain_Amygdala
Esophagus_Mucosa
Brain_Substantia_nigra
Testis
Brain_Spinal_cord_cervical_c-1
Pancreas
Esophagus_Gastroesophageal_Junction
Ovary
Skin_Sun_Exposed_Lower_leg
Lung
study
−0.8 −0.6 −0.4 −0.2 0.0 0.2 0.4 0.6 0.8
effect size

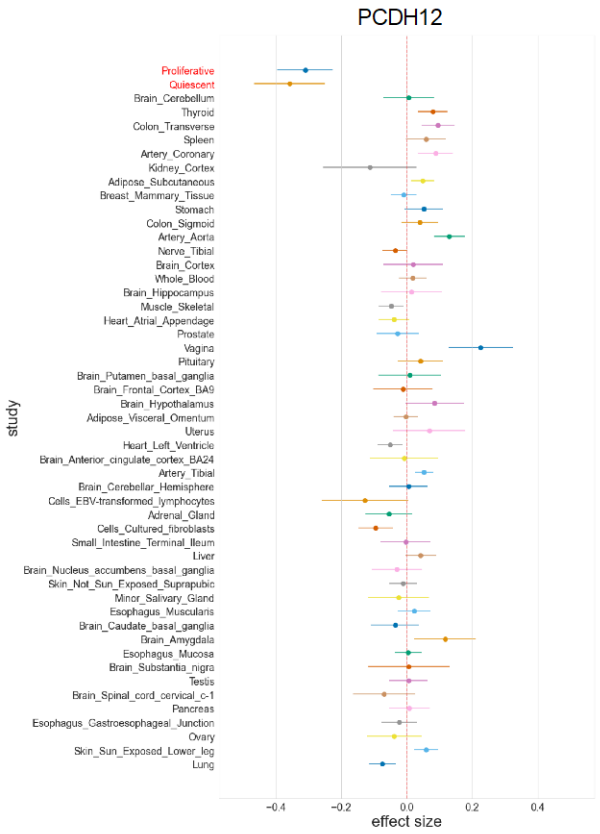
PCDH12
study
Proliferative
Quiescent
Brain_Cerebellum
Thyroid
Colon_Transverse
Spleen
Artery_Coronary
Kidney_Cortex
Adipose_Subcutaneous
Breast_Mammary_Tissue
Stomach
Colon_Sigmoid
Artery_Aorta
Nerve_Tibial
Brain_Cortex
Whole_Blood
Brain_Hippocampus
Muscle_Skeletal
Heart_Atrial_Appendage
Prostate
Vagina
Pituitary
Brain_Putamen_basal_ganglia
Brain_Frontal_Cortex_BA9
Brain_Hypothalamus
Adipose_Visceral_Omentum
Uterus
Heart_Left_Ventricle
Brain_Anterior_cingulate_cortex_BA24
Artery_Tibial
Brain_Cerebellar_Hemisphere
Cells_EBV-transformed_lymphocytes
Adrenal_Gland
Cells_Cultured_fibroblasts
Small_Intestine_Terminal_Ileum
Liver
Brain_Nucleus_accumbens_basal_ganglia
Skin_Not_Sun_Exposed_Suprapubic
Minor_Salivary_Gland
Esophagus_Muscularis
Brain_Caudate_basal_ganglia
Brain_Amygdala
Esophagus_Mucosa
Brain_Substantia_nigra
Testis
Brain_Spinal_cord_cervical_c-1
Pancreas
Esophagus_Gastroesophageal_Junction
Ovary
Skin_Sun_Exposed_Lower_leg
Lung
−0.4
−0.2
0.0
0.2
0.4
effect size

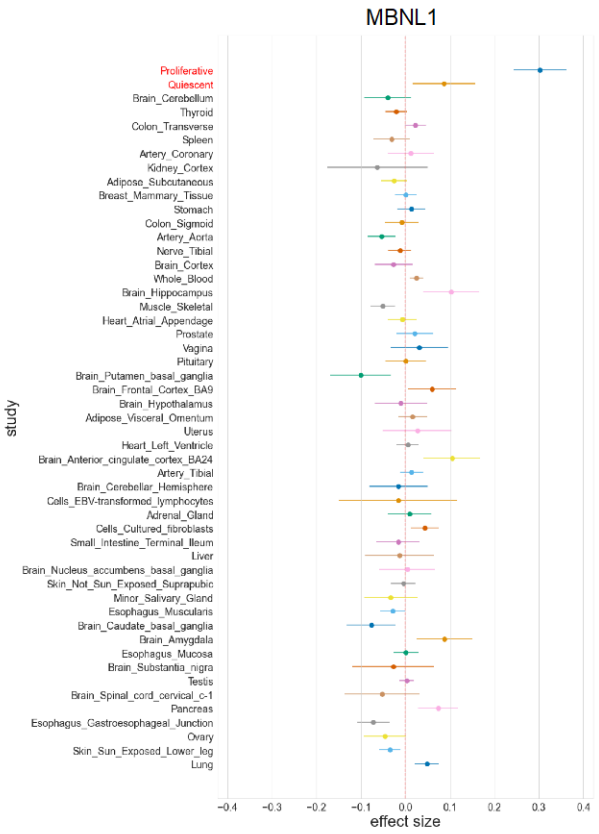
MBNL1
study
Proliferative
Quiescent
Brain_Cerebellum
Thyroid
Colon_Transverse
Spleen
Artery_Coronary
Kidney_Cortex
Adipose_Subcutaneous
Breast_Mammary_Tissue
Stomach
Colon_Sigmoid
Artery_Aorta
Nerve_Tibial
Brain_Cortex
Whole_Blood
Brain_Hippocampus
Muscle_Skeletal
Heart_Atrial_Appendage
Prostate
Vagina
Pituitary
Brain_Putamen_basal_ganglia
Brain_Frontal_Cortex_BA9
Brain_Hypothalamus
Adipose_Visceral_Omentum
Uterus
Heart_Left_Ventricle
Brain_Anterior_cingulate_cortex_BA24
Artery_Tibial
Brain_Cerebellar_Hemisphere
Cells_EBV-transformed_lymphocytes
Adrenal_Gland
Cells_Cultured_fibroblasts
Small_Intestine_Terminal_Ileum
Liver
Brain_Nucleus_accumbens_basal_ganglia
Skin_Not_Sun_Exposed_Suprapubic
Minor_Salivary_Gland
Esophagus_Muscularis
Brain_Caudate_basal_ganglia
Brain_Amygdala
Esophagus_Mucosa
Brain_Substantia_nigra
Testis
Brain_Spinal_cord_cervical_c-1
Pancreas
Esophagus_Gastroesophageal_Junction
Ovary
Skin_Sun_Exposed_Lower_leg
Lung
−0.4
−0.3
−0.2
−0.1
0.0
0.1
0.2
0.3
0.4
effect size


RANBP3
study
Proliferative
Quiescent
Brain_Cerebellum
Thyroid
Colon_Transverse
Spleen
Artery_Coronary
Kidney_Cortex
Adipose_Subcutaneous
Breast_Mammary_Tissue
Stomach
Colon_Sigmoid
Artery_Aorta
Nerve_Tibial
Brain_Cortex
Whole_Blood
Brain_Hippocampus
Muscle_Skeletal
Heart_Atrial_Appendage
Prostate
Vagina
Pituitary
Brain_Putamen_basal_ganglia
Brain_Frontal_Cortex_BA9
Brain_Hypothalamus
Adipose_Visceral_Omentum
Uterus
Heart_Left_Ventricle
Brain_Anterior_cingulate_cortex_BA24
Artery_Tibial
Brain_Cerebellar_Hemisphere
Cells_EBV-transformed_lymphocytes
Adrenal_Gland
Cells_Cultured_fibroblasts
Small_Intestine_Terminal_Ileum
Liver
Brain_Nucleus_accumbens_basal_ganglia
Skin_Not_Sun_Exposed_Suprapubic
Minor_Salivary_Gland
Esophagus_Muscularis
Brain_Caudate_basal_ganglia
Brain_Amygdala
Esophagus_Mucosa
Brain_Substantia_nigra
Testis
Brain_Spinal_cord_cervical_c-1
Pancreas
Esophagus_Gastroesophageal_Junction
Ovary
Skin_Sun_Exposed_Lower_leg
Lung
−0.4
−0.3
−0.2
−0.1
0.0
0.1
0.2
0.3
0.4
effect size

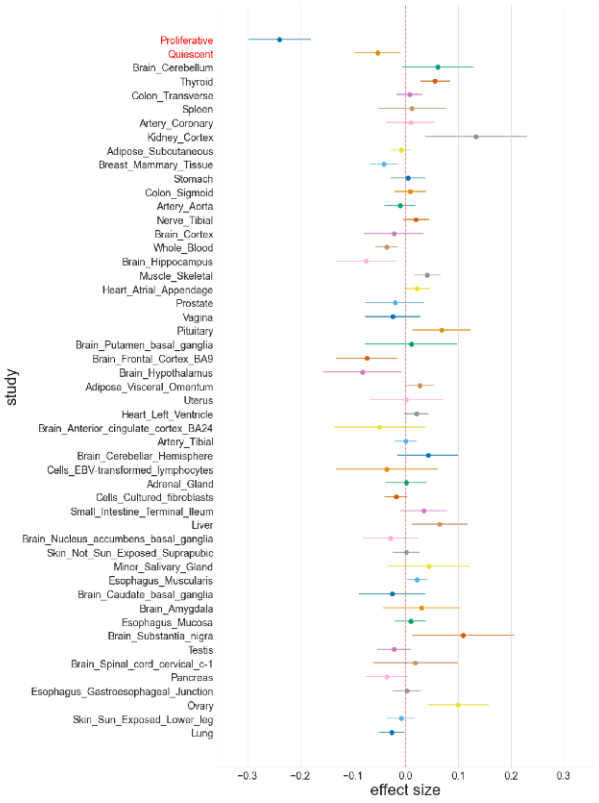
TFDP2
study
Proliferative
Quiescent
Brain_Cerebellum
Thyroid
Colon_Transverse
Spleen
Artery_Coronary
Kidney_Cortex
Adipose_Subcutaneous
Breast_Mammary_Tissue
Stomach
Colon_Sigmoid
Artery_Aorta
Nerve_Tibial
Brain_Cortex
Whole_Blood
Brain_Hippocampus
Muscle_Skeletal
Heart_Atrial_Appendage
Prostate
Vagina
Pituitary
Brain_Putamen_basal_ganglia
Brain_Frontal_Cortex_BA9
Brain_Hypothalamus
Adipose_Visceral_Omentum
Uterus
Heart_Left_Ventricle
Brain_Anterior_cingulate_cortex_BA24
Artery_Tibial
Brain_Cerebellar_Hemisphere
Cells_EBV-transformed_lymphocytes
Adrenal_Gland
Cells_Cultured_fibroblasts
Small_Intestine_Terminal_Ileum
Liver
Brain_Nucleus_accumbens_basal_ganglia
Skin_Not_Sun_Exposed_Suprapubic
Minor_Salivary_Gland
Esophagus_Muscularis
Brain_Caudate_basal_ganglia
Brain_Amygdala
Esophagus_Mucosa
Brain_Substantia_nigra
Testis
Brain_Spinal_cord_cervical_c-1
Pancreas
Esophagus_Gastroesophageal_Junction
Ovary
Skin_Sun_Exposed_Lower_leg
Lung
−0.3
−0.2
−0.1
0.0
0.1
0.2
0.3
effect size

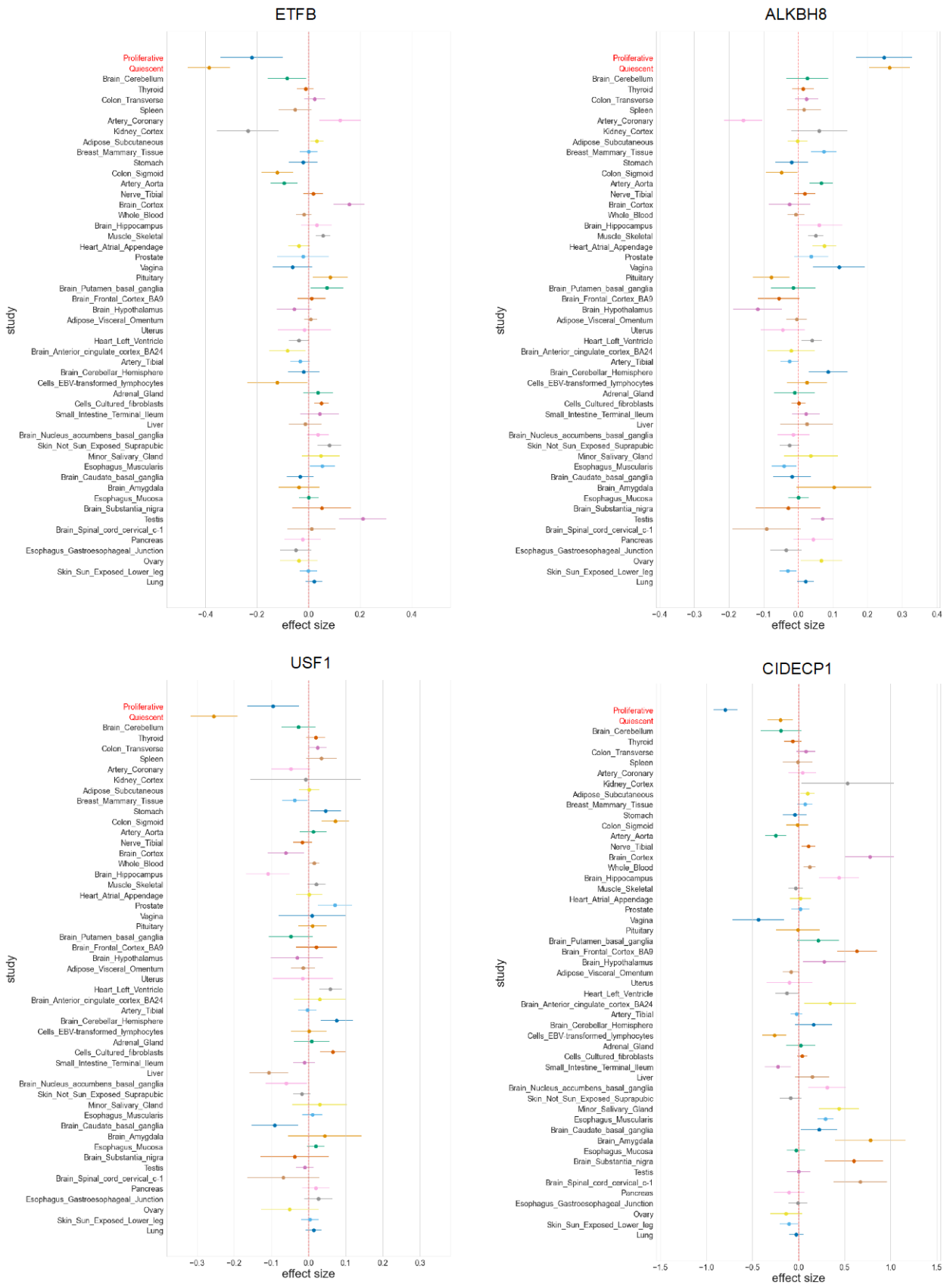
ETFB
ALKBH8
USF1
CIDECP1
study
effect size
Proliferative
Quiescent
Brain_Cerebellum
Thyroid
Colon_Transverse
Spleen
Artery_Coronary
Kidney_Cortex
Adipose_Subcutaneous
Breast_Mammary_Tissue
Stomach
Colon_Sigmoid
Artery_Aorta
Nerve_Tibial
Brain_Cortex
Whole_Blood
Brain_Hippocampus
Muscle_Skeletal
Heart_Atrial_Appendage
Prostate
Vagina
Pituitary
Brain_Putamen_basal_ganglia
Brain_Frontal_Cortex_BA9
Brain_Hypothalamus
Adipose_Visceral_Omentum
Uterus
Heart_Left_Ventricle
Brain_Anterior_cingulate_cortex_BA24
Artery_Tibial
Brain_Cerebellar_Hemisphere
Cells_EBV-transformed_lymphocytes
Adrenal_Gland
Cells_Cultured_fibroblasts
Small_Intestine_Terminal_Ileum
Liver
Brain_Nucleus_accumbens_basal_ganglia
Skin_Not_Sun_Exposed_Suprapubic
Minor_Salivary_Gland
Esophagus_Muscularis
Brain_Caudate_basal_ganglia
Brain_Amygdala
Esophagus_Mucosa
Brain_Substantia_nigra
Testis
Brain_Spinal_cord_cervical_c-1
Pancreas
Esophagus_Gastroesophageal_Junction
Ovary
Skin_Sun_Exposed_Lower_leg
Lung

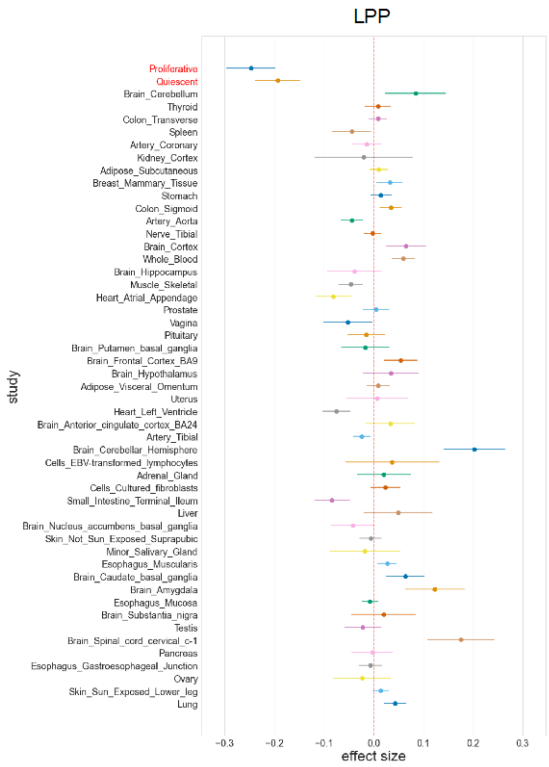

Supplementary Figure 5: SMC-specific eQTLs. SMC-specific eQTLs were identified using METASOFT. 29 SMC-specific eQTLs were defined by SNP-gene pairs with posterior probability (METASOFT M-value) > 0.9 in SMCs and < 0.1 in all the GTEx tissues and cells. The plots show the comparison of the effect sizes of SMC-specific eQTLs and 49 GTEx tissues and cells. Error bar indicates 95% confidence intervals.

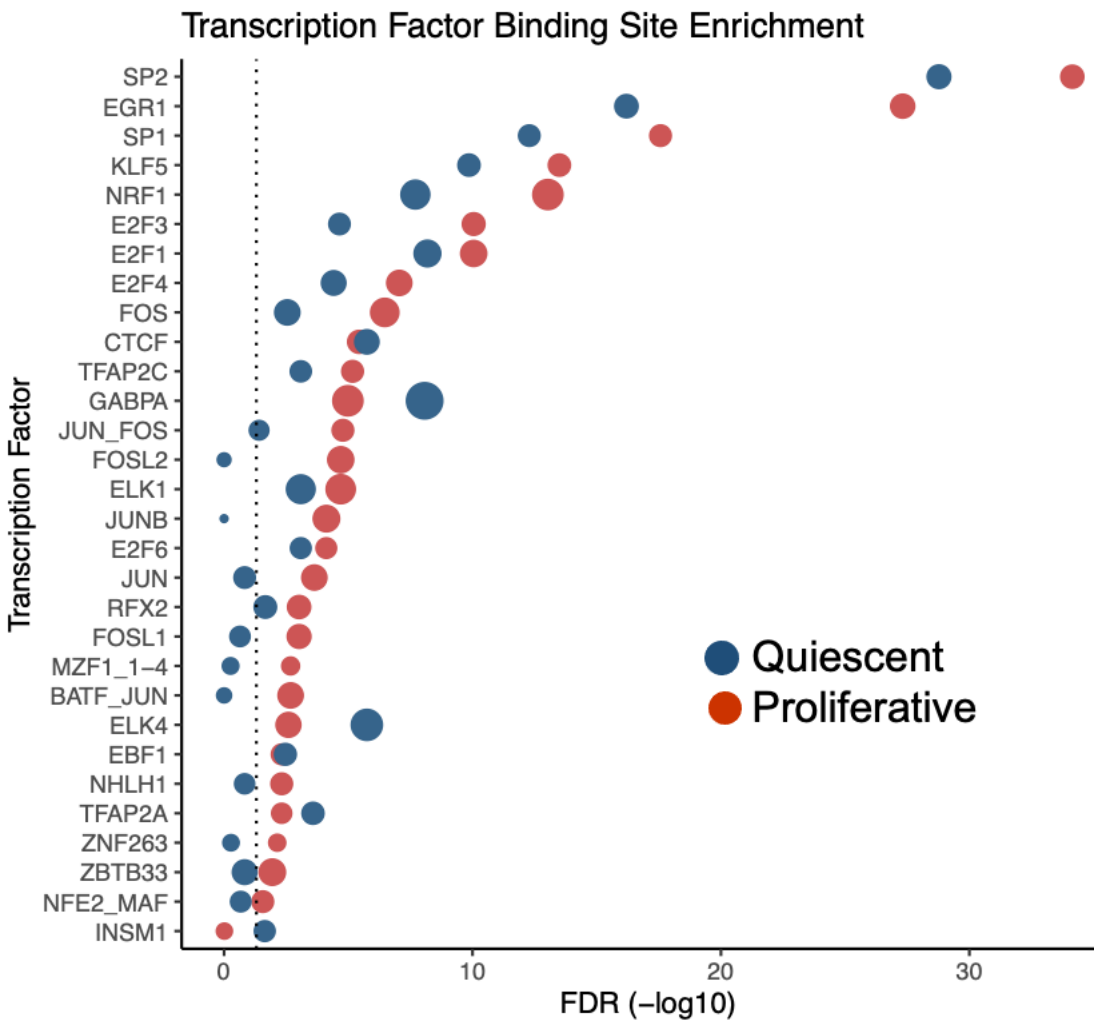

Supplementary Figure 6: Identification of transcription factors overlapping SMC *cis*-eQTLs. SMC *cis*-eQTL SNPs and their LD proxies in accessible chromatin regions were interrogated for overlap for putative transcription factor (TF) binding sites using SNP2TFBS. The TF enrichment values were calculated as the ratio of the observed SNP hits over the expected ones for each TF. The statistical significance of the enrichment was calculated using a binomial test and corrected for multiple testing using the qvalue package in R. The plot shows TFs ranked according to their FDR q-values for both quiescent and proliferative SMCs. The point size is proportional to the TF enrichment.

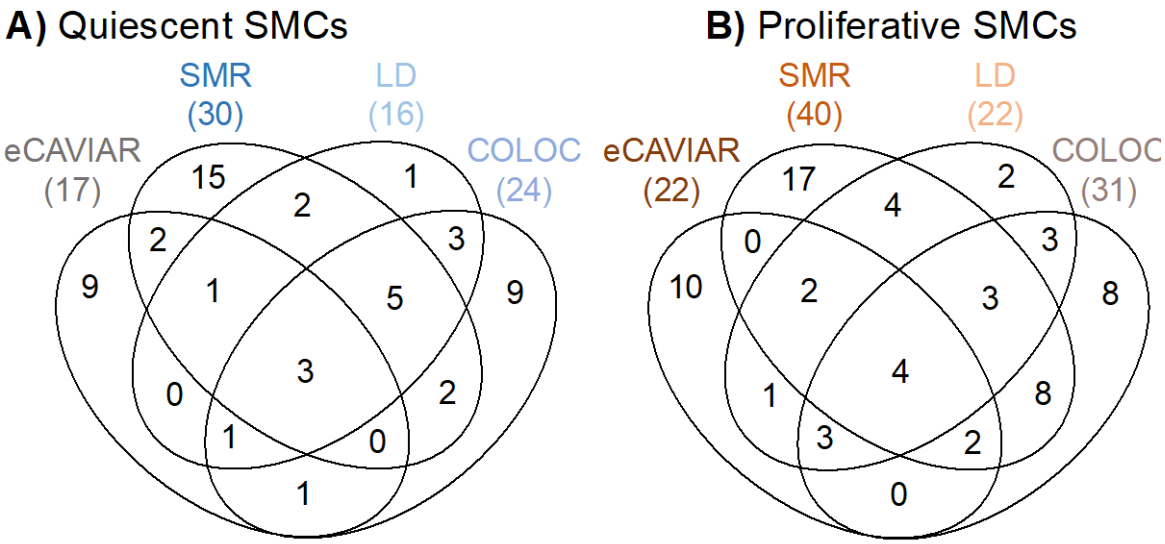

Quiescent (17)	Both (37)		Proliferative (30)	
AL513548.3[E,C,L,S]	AL592148.3[E]	LMAN1[E]	AC009054.2[L,S]	PDGFD[C]
CCDC158[C]	ARHGAP42[C,S]	MAP1S[C]	ADAMTS7[S]	PSD4[E]
HLA-B[S]	ARVCF[E]	MARCH2[E,C,S]	AP003392.4[E,L]	SKIV2L[S]
ILF3-AS1[S]	CFDP1[C,L,S]	MLH3[C,L,S]	ATP5MC1[S,L]	SLC2A12[S]
IQGAP1[C]	CGGBP1[E]	MRPL45P2[S]	CD109[E]	SMAD3[E,C,L,S]
LIPG[C]	DAGLB[C,L,S]	NEK9[C,L,S]	CDK8[E]	STAT6[C,L]
MACC1[E]	DDX59-AS1[C,E,L]	NME6[S]	CETP[C,L]	TCEA2[E,L,S]
PIK3CB[S]	DHODH[S]	REST[E,C,L,S]	CTSK[C]	TMEM106B[C]
PSMA3-AS1[C,L]	DHX38[C,L,S]	RGS19[L]	CTSS[S]	TMEM91[S]
RCCD1[C]	EFCAB5[C,S]	RIC8A[E]	DHX58[C]	TRIP4[L]
RP11-731C17.2[S]	EIF2B2[E,C,L,S]	RP11-33B1.1[S]	FURIN[E,C,L,S]	
RRP1B[E]	ERAP2[E,S]	SNHG18[C,L]	GOLPH3L[C,S]	
SERPINF1[S]	FES[E,C,L,S]	SORBS2[E,L,S]	HAUS4[S]	
SMG6[S]	FGD6[E,C,S]	TDRKH-AS1[E,C,L]	IRAK1BP1[E]	
THOC5[S]	FHL3[C,L,S]	TOM1L2[C,S]	LINC02542[C,S]	
TMEM87B[S]	GSTT2B[S]	ZFP30[S]	LNPEP[S]	
YEATS4[E]	GTF2IP12[C]	ZNF100[E,S]	MAP3K7CL[E,C,L,S]	
	HMBS[L,S]		NAGLU[S]	
	INPP5B[C]		NME7[C,S]	
	KIAA0040[E]		NPHP3[S]	

[E] eCAVIAR , [C] COLOC, [L] LD, [S] SMR

Supplementary Figure 7: Summary of the four different approaches used to perform SMC eQTL and CAD GWAS colocalization. 1) eQTLs identified in quiescent and proliferative SMCs were colocalized based on linkage disequilibrium of the CAD index SNP and the most significantly associated eQTL SNP (LD). **2)** They were also colocalized using Summary Level Mendelian Randomization (SMR) to test for the pleiotropic association of gene expression in SMCs and CAD. **3)** eQTL and GWAS CAusal Variants Identification in Associated Regions (eCAVIAR) was used to test for causal SNPs between SMC eQTLs and the CAD GWAS. **4)** Bayesian Colocalization Analysis (COLOC) was used to identify the colocalization between SMC eQTLs and the CAD GWAS. The letters in superscript for each gene indicate the approach where the evidence for the colocalization comes from.

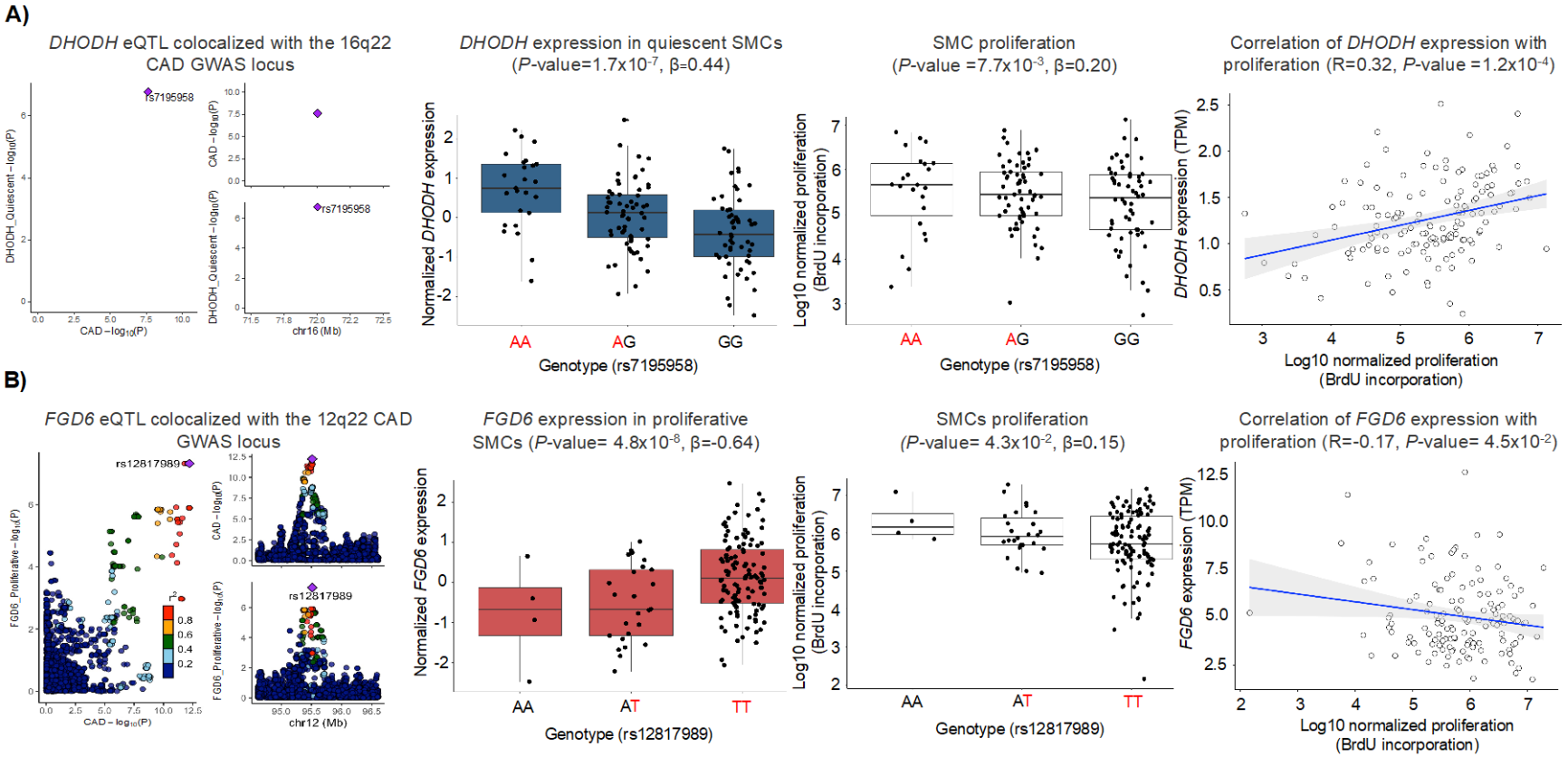

Supplementary Figure 8: Association of CAD colocalized SMC cis-eQTLs with atherosclerosis-relevant SMC phenotypes. A) *DHODH cis*-eQTL colocalized with the 16q22 CAD GWAS locus (left), the risk allele, A, of the SNP rs7195958 is associated with higher *DHODH* expression in quiescent SMCs and also SMC proliferation. We observed significant positive correlation between *DHODH* expression and SMC proliferation (right). **B)** *FGD6 cis*-eQTL signal colocalized with the 12q22 CAD GWAS locus (left), the risk allele, T, of the SNP rs12817989 is associated with higher *FGD6* expression in proliferative SMCs and lower proliferation. We observed a significant negative correlation between *FGD6* expression and SMC proliferation (right).

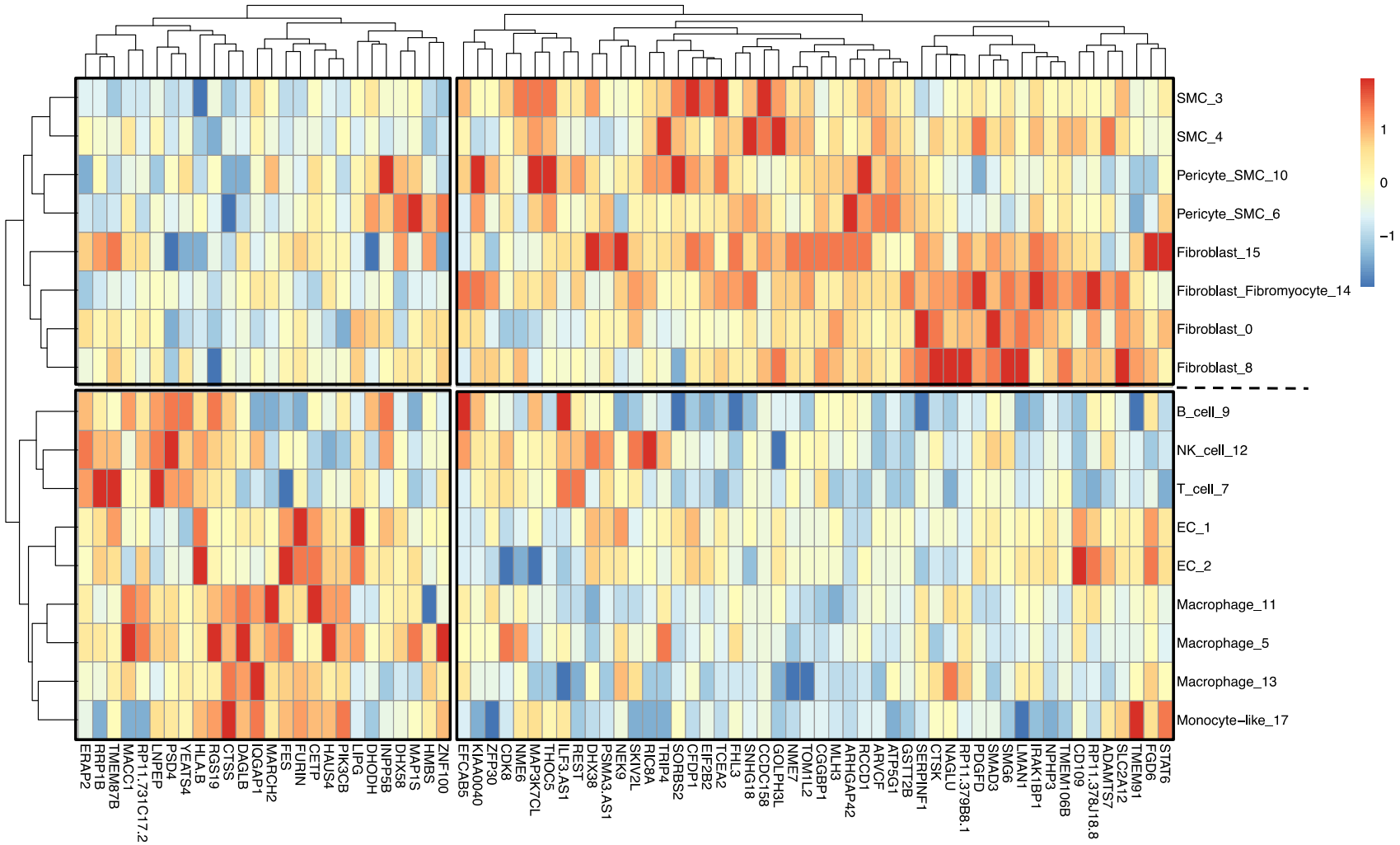

Supplementary Figure 9: SMC eQTL gene expression in single cells isolated from human coronary atherosclerotic plaques. The scRNAseq data has been published previously[70]. We were able to assess the expression of 76 of the 84 SMC eQTL genes colocalized with CAD loci. 50 of the 76 genes had higher expression in SMCs, pericytes, and fibroblasts compared to endothelial cells, monocytes, macrophages, and other immune cells. The color key of the amount of expression ranging from −2 (blue) to +2 (red) is shown on the right. Red color indicates higher expression, while blue color indicates lower expression.

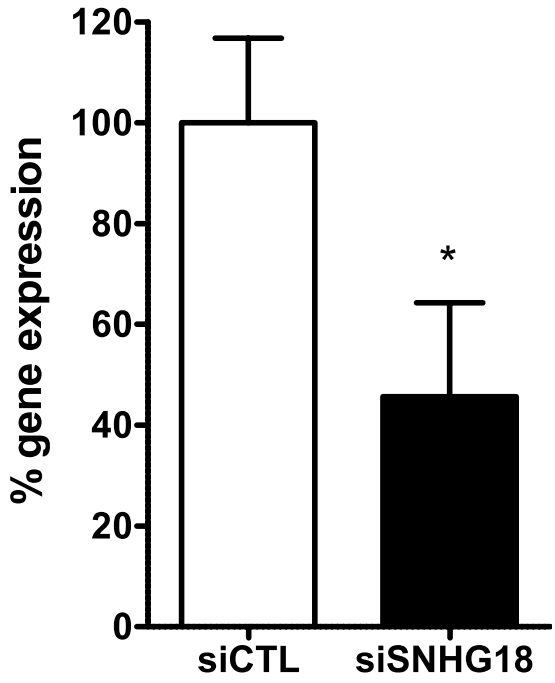

Supplementary Figure 10: qPCR results after SNHG18 downregulation in SMCs. SMCs were transfected with control siRNA, and SNHG18 siRNA and qPCR analyses were conducted 48 hours post-transfection. * $p<0.05$.

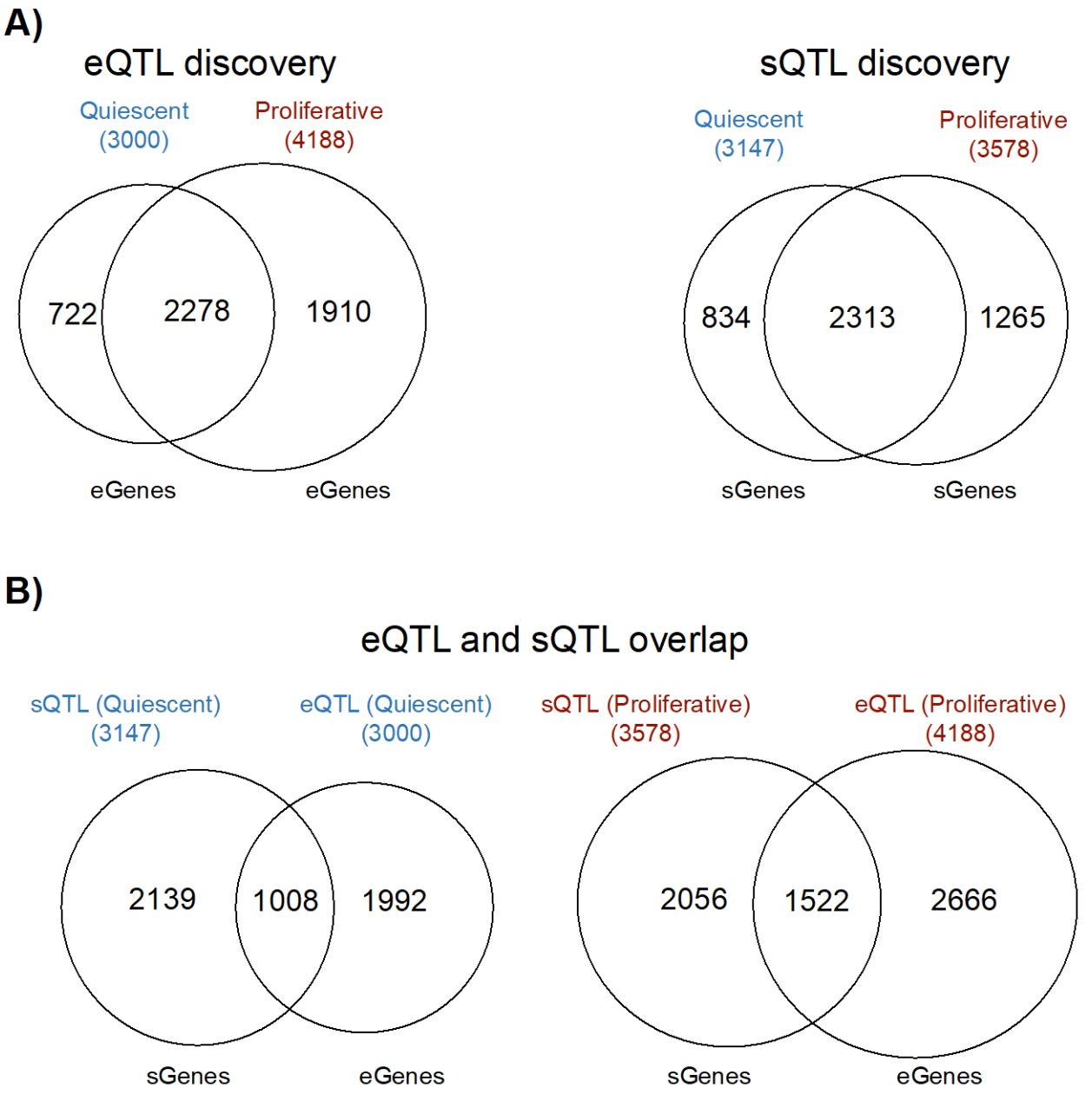

Supplementary Figure 11: Number of eGenes and sGenes discovered in quiescent and proliferative SMCs. A) Comparison of the number of eGenes and sGenes discovered in quiescent and proliferative SMCs showed a large overlap between the phenotypes (Poverlap $<1x10^{-300}$, hypergeometric test for both eQTL and sQTL). **B)** Overlap of genes with an eQTL or sQTL ($P_{overlap} = 4.7x10^{-136}$, hypergeometric test for quiescent SMCs and ($P_{overlap} = 9.1x10^{-189}$, hypergeometric test for proliferative SMCs) showed that genetic regulation of the expression or splicing of mRNAs was largely independent.

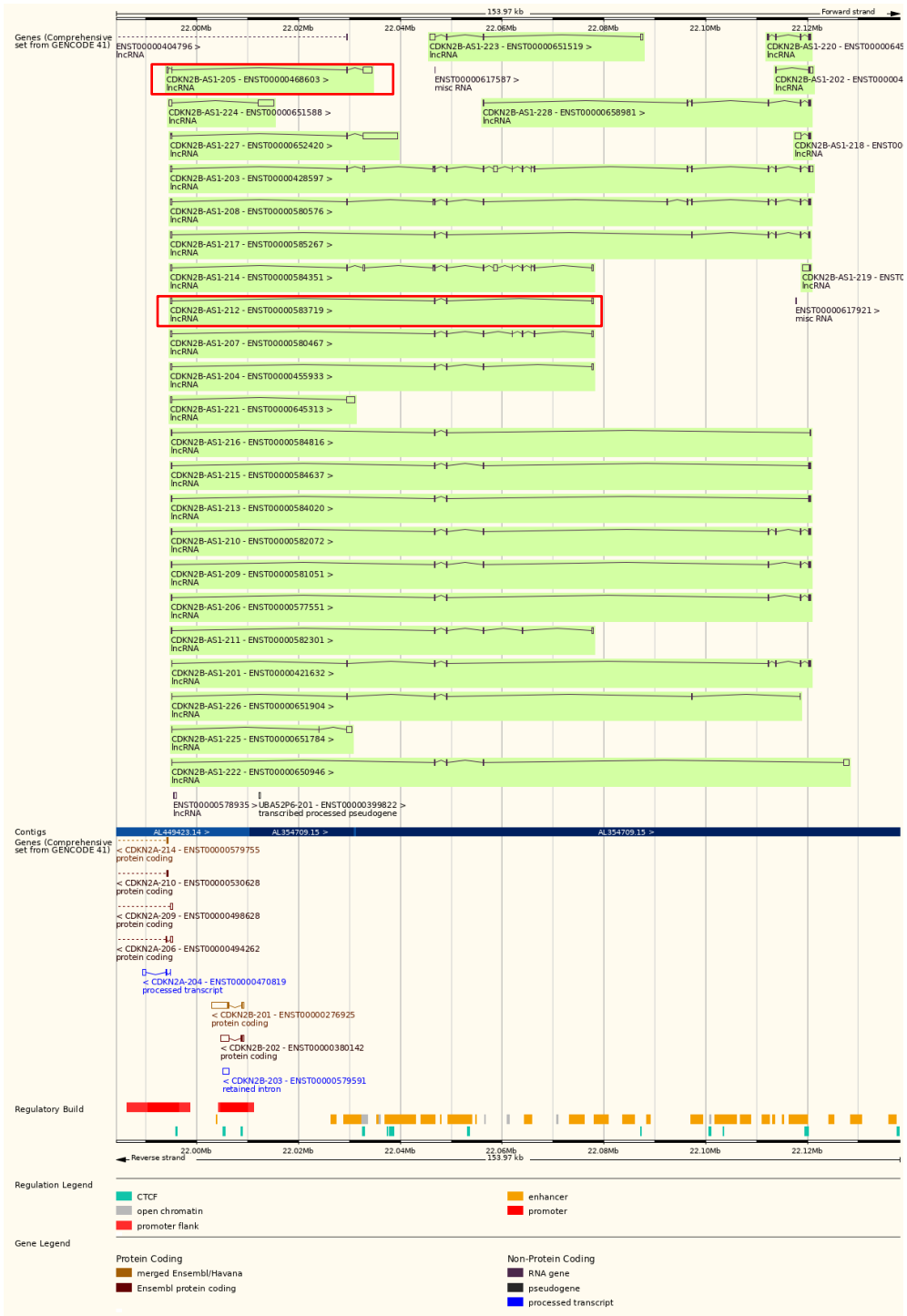

Supplementary Figure 12: Human CDKN2B-AS1 transcripts structure from Ensembl Genome Browser (GRCh38.p13). The isoform structures of the two most abundant transcripts are highlighted with red boxes.